A&A 639, A4 (2020)
https://doi.org/10.1051/0004-6361/202037497

Astronomy & Astrophysics

Infrared spectra of complex organic molecules in astronomically relevant ice mixtures

II. Acetone

M. G. Rachid[1], J. Terwisscha van Scheltinga[1,2], D. Koletzki[1,⋆], and H. Linnartz[1]

[1] Laboratory for Astrophysics, Leiden Observatory, Leiden University, PO Box 9513, 2300 RA Leiden, The Netherlands
e-mail: marina.g.rachid@gmail.com
[2] Leiden Observatory, Leiden University, PO Box 9513, 2300 RA Leiden, The Netherlands

Received 14 January 2020 / Accepted 28 February 2020

ABSTRACT

Context. Complex organic molecules (COMs) have been largely identified through their characteristic rotational transitions in the gas of interstellar and circumstellar regions. Although these species are formed in the icy mantles that cover dust grains, the most complex species that has been unambiguously identified in the solid-phase to date is methanol (CH_3OH). With the upcoming launch of the *James Webb* Space Telescope (JWST), this situation may change. The higher sensitivity, spectral and spatial resolution of the JWST will allow for the probing of the chemical inventory of ices in star-forming regions. In order to identify features of solid-state molecules in astronomical spectra, laboratory infrared spectra of COMs within astronomically relevant conditions are required. This paper is part of a series of laboratory studies focusing on the infrared spectra of frozen COMs embedded in ice matrices. These reflect the environmental conditions in which COMs are thought to be found.

Aims. This work is aimed at characterizing the infrared features of acetone mixed in ice matrices containing H_2O, CO_2, CO, CH_4, and CH_3OH for temperatures ranging between 15 K and 160 K. Changes in the band positions and shapes due to variations in the temperature, ice composition, and morphology are reported. This work also points out the IR features that are considered the best promising tracers when searching for interstellar acetone-containing ices.

Methods. Acetone-containing ices were grown at 15 K under high-vacuum conditions and infrared (IR) spectra (500–4000 cm^{-1}/20–2.5 μm, 0.5 cm^{-1} resolution) in transmission mode were recorded using a Fourier transform infrared spectrometer. Spectra of the ices at higher temperatures are acquired during the heating of the sample (at a rate of 25 K h^{-1}) up to 160 K. The changes in the infrared features for varying conditions were analyzed.

Results. A large set of IR spectra of acetone-containing ices is presented and made available as a basis for interpreting current and future infrared astronomical spectra. The peak position and full width at half maximum of selected acetone bands have been measured for different ice mixtures and temperatures. The bands that are best suitable for acetone identification in astronomical spectra are: the C=O stretch mode, around 1710.3 cm^{-1} (5.847 μm), that lies in the 1715–1695 cm^{-1} (5.83–5.90 μm) range in the mixed ices; the CH_3 symmetric deformation, around 1363.4 cm^{-1} (7.335 μm) that lies in the 1353–1373 cm^{-1} (7.28–7.39 μm) range in the mixed ices; and the CCC asymmetric stretch, around 1228.4 cm^{-1} (8.141 μm), that lies in the 1224–1245 cm^{-1} (8.16–8.03 μm) range in the mixed ices. The CCC asymmetric stretch band also exhibits potential as a remote probe of the ice temperature and composition; this feature is the superposition of two components that respond differently to temperature and the presence of CH_3OH. All the spectra are available through the Leiden Ice Database.

Key words. astrochemistry – molecular data – methods: laboratory: molecular – ISM: molecules – methods: laboratory: solid state

1. Introduction

The increasing number of molecules detected outside our Solar System directly correlates to the many chemical processes taking place in space. Up through today, more than 225 different molecules have been identified in the interstellar medium (McGuire 2018). The majority of these species have typical sizes ranging up to 13 atoms, and a few much larger molecules have also been identified in space: such as the fullerenes C_{60}, C_{60}^+, and C_{70}, (Cami et al. 2010; Sellgren et al. 2010; Berné et al. 2013; Campbell et al. 2015; Cordiner et al. 2019). These molecules have been detected across a diversity of environments (diffuse and cold molecular clouds, circumstellar disks and gas shells expelled by stars at the end of their lives) (Ehrenfreund & Charnley 2000). Most of these species have been identified exclusively through their gas-phase signatures; only some 12 species have been found in the solid-state and among these, the only complex organic molecule (COM) that has been definitively detected is methanol (CH_3OH). As it is generally thought that COMs form through surface induced reactions (Herbst & Van Dishoeck 2009; Linnartz et al. 2015; Öberg 2016), the lack of astronomical solid-state COMs identifications calls for further attention.

Infrared observational data have shown that the icy material in cold regions of dark clouds and protoplanetary disks can harbour simple molecules, such as H_2O, CO, CO_2, NH_3, CH_4, and CH_3OH (Gibb et al. 2004; Öberg et al. 2011; Boogert et al. 2015). Laboratory work has shown that many COMs can be formed starting from these simple precursor molecules,

⋆ Current address: Technische Universiteit Delft, Mekelweg 5, 2628 CD Delft, The Netherlands.

either through non-energetic processing, such as atom or radical addition and recombination reactions (Watanabe & Kouchi 2002; Ioppolo et al. 2011; Fedoseev et al. 2015; Linnartz et al. 2015), or energetic processing, for example, via irradiation by UV photons, cosmic-rays, and electrons (Gerakines et al. 1996; Hudson & Moore 1999, 2001; Öberg et al. 2009; Duarte et al. 2010). With the upcoming launch of the *James Webb* Space Telescope (JWST), spatially, and spectroscopically well-resolved infrared spectra of ices in star-forming regions will become available. Within ICE AGE[1], an early release JWST science program, efforts have been underway to search for the solid-state signatures of larger and more complex species, COMs in particular, that may play a role in the formation of the building blocks of life. In order to identify the infrared features of COMs in the astronomical data, reference spectra in simulated space environments are required. Currently, worldwide efforts are made to have these data available in time. This paper deals with ices containing acetone (CH_3COCH_3).

Acetone was detected in the interstellar medium (ISM) for the first time in the hot molecular core Sgr B2 (Combes et al. 1987; Snyder et al. 2002). Since then, it has also been detected in other high mass star forming regions (Friedel et al. 2005; Zou & Weaver 2017), towards an intermediate-mass protostar (Fuente et al. 2014), the low mass protostar IRAS 16293−2422B (Lykke et al. 2017) and in the disk around the outbursting star V883 Ori (Lee et al. 2019). Acetone is a key molecule to understand the O–N differentiation in the Orion-KL region. There, large N-bearing molecules and large O-bearing molecules are spatially separated. The presence of acetone in both these chemically different environments, indicates that this species may have a unique formation mechanism, that is expected to follow solid-state routes (Friedel & Snyder 2008; Zou & Weaver 2017).

Initially, the formation of acetone in the ISM was proposed to occur by the radiative association of a methyl ion and acetaldehyde in the gas-phase resulting in the formation of protonated acetone ($CH_3COCH_3^+$) that sequentially recombines with electrons to form neutral acetone (Combes et al. 1987):

$$CH_3^+ + CH_3CHO \rightarrow CH_3COCH_3^+ + h\nu$$

$$CH_3COCH_3^+ + e^- \rightarrow CH_3COCH_3.$$

Herbst et al. (1990) carried out a theoretical study of acetone formation through ion-molecule reactions and demonstrated that the reaction between the methyl ion and acetaldehyde proposed by Combes et al. (1987) is not efficient enough to account for the observed CH_3COCH_3 abundances in Sgr B2. Instead, the authors proposed that acetone synthesis could involve surface chemistry pathways, a proposition that is observationally supported by the recent work by Lee et al. (2019).

Garrod et al. (2008) proposed that the solid state formation of some COMs, including acetone, in hot cores could happen through the reaction between aldehyde-group radicals and primary or secondary radicals in ice grain mantles:

$$CH_3CHO + CH_3 \rightarrow CH_3CO + CH_4,$$

$$CH_3CO + CH_3 \rightarrow CH_3COCH_3.$$

Later, the formation of acetone and acetaldehyde in $CO:CH_4$ ices irradiated by 5 keV electrons was confirmed by Kaiser et al. (2014). An unambiguous identification of acetone in the solid-state would, therefore, shed further light on its chemical origin in ISM.

Hudson et al. (2018) reported IR spectra of amorphous and crystalline acetone ice, at 10 K and 125 K, respectively. The authors compared their reported data with spectra available in the literature, characterized the changes in shape and band position in the acetone spectra at different temperatures, deposition conditions and thicknesses, and reported refractive index, density and band strength values for the vibrational modes for both amorphous and crystalline acetone ices. In order to further support the interpretation of infrared astronomical data, it is important to extend studies of pure acetone ice to acetone-containing ice mixtures comprising abundant interstellar ice species or species that are considered likely precursors of solid-state acetone. Moreover, such spectra need to be recorded for different temperatures and ice growth conditions as vibrational modes are affected by the chemical composition, temperature, and physical structure of the ice (Palumbo 2005; Dawes et al. 2007; Öberg et al. 2007; Bossa et al. 2012; Isokoski et al. 2014), causing peak positions, peak shapes (e.g., the full width at half maximum, FWHM), and intensity ratios to vary for different experimental settings. Adding to this, vibrational modes may absorb at wavelengths overlapping with those of similar functional groups from other molecules in the ice, which will further complicate unambiguous infrared identifications.

This work presents a study of the infrared spectral features of acetone in its pure form and mixed in relevant interstellar ice matrices: H_2O, CO, CH_3OH, CO_2, $H_2O:CO_2$, $H_2O:CH_4$, and $CO:CH_3OH$. The strongest bands of acetone ($A > 10^{-18}$ cm molecule^{-1} from Hudson et al. 2018) have been selected and are characterized in terms of peak position, FWHM, and band intensity ratios. The decision to focus on the strongest bands is based on the fact that those are most suited to act as acetone tracers in astronomical infrared spectra.

The present paper is structured as follows: Sect. 2 describes the apparatus and the measurement protocols. In Sect. 3, the results of selected spectral features of acetone in different mixtures are presented and the astronomical importance of the present measurements is discussed. The conclusions are outlined in Sect. 4. Selected wavelength domains of the infrared spectra of all the samples studied in this work, along with graphs showing the peak position versus FWHM and the calculated apparent band strengths, are summarized in Appendix A. The tables listing peak positions and FWHM values for all the studied bands are listed in Appendix B. The integrated absorbance of the different acetone bands is summarized in Appendix C.

2. Methodology

All the measurements are performed in a high-vacuum (HV) setup with a central stainless steel chamber with a base pressure of $\sim 3 \times 10^{-7}$ mbar and which houses a cryogenically cooled IR transparent window (ZnSe) onto which ices are grown. The pressure in the main chamber is measured using a full range pressure gauge. The liquids and gases used in the preparation of the gas mixtures are acetone (Roth, purity ≥99.9%), water (Milli-Q, Type I), carbon monoxide (Linde Gas, 99.997%), methane (Linde Gas 99.999%), and methanol (Honeywell, purity ≥99.9%). The gas samples, pure and mixed, are prepared in a separate mixing line using a 2 L glass bulb

[1] http://jwst-iceage.org/

Table 1. Composition, mixing ratios and temperature range of the analyzed ice samples.

Mixture	1:5	1:20	Temperature range (K)
CH_3COCH_3:H_2O	1:5	1:20	15–160
CH_3COCH_3:CO_2	1:5	1:20	15–100
CH_3COCH_3:H_2O:CO_2	1:2.5:2.5	1:10:10	15–160
CH_3COCH_3:H_2O:CH_4	1:2.5:2.5	1:10:10	15–160
CH_3COCH_3:CH_3OH	1:5	1:20	15–140
CH_3COCH_3:CO	1:5	1:20	15–35
CH_3COCH_3:CH_3OH:CO	1:2.5:2.5	1:10:10	15–140

Notes. Uncertainty in the mixing ratios due to preparation of the sample is lower than 10%.

typically filled up to a total pressure of 20 mbar. The mixtures are prepared through the sequential freezing of gases in the glass bulb immersed in a liquid N_2 bath. The base pressure in the mixing line is around 1×10^{-4} mbar and measured using two mass-independent pressure gauges that cover ranges between 0−10 mbar and 0−1000 mbar. The estimated error in the mixing ratios obtained by this method is ≤10%. The gas sample is admitted into the main chamber through an inlet valve and the flow is controlled by a calibrated needle valve that is maintained at the same fixed position for all the experiments. The gases are background deposited onto the cryogenically cooled (15 K) ZnSe window using a closed cycle He cryostat. The sample temperature is monitored using a silicon diode DT-670-CU, PID controlled by a Lake Shore 330 temperature controller, with an absolute accuracy of 2 K and a relative accuracy of 1 K. In this work, the needle valve has already been calibrated for different pure gases, enabling the calculation of their deposition rate (the band strengths for the quantification were taken from Bouilloud et al. 2015; Hudson et al. 2018). Taking into account the deposition rate of pure gases weighted by their respective fraction in the desired gas mixtures, it becomes possible to determine the deposition rate of the gas mixtures. Consequently, the column density of each component in the ice can be calculated. Once the column density of acetone and the integrated IR absorption of a given vibrational mode are known, it is possible to calculate the apparent band strength of an acetone band for a specific ice mixture and temperature.

The ice samples are typically grown over a period of 30 min, resulting in an ice thickness between 2800 ML and 3500 ML (1 ML ∼ 1×10^{15} molecules cm^{-2}), depending on the composition of the gas mixture. These thick ices are used to minimize the influence of contamination from the background gases, which is mainly water at a measured rate of 30 ML h^{-1}. As a control, it is checked that the C=O stretching band signal does not saturate during mixture deposition. The infrared beam of a Varian 670-IR infrared spectrometer is guided perpendicularly through the substrate to obtain the IR spectra of the ice samples in transmission mode. The spectrometer covers a range between 4000 cm^{-1} and 500 cm^{-1} (2.5–20 μm) at spectral resolutions as high as 0.1 cm^{-1}. In this work, the spectra are collected using a resolution of 0.5 cm^{-1}. All the recorded spectra are averaged over 128 scans (around 3.5 min). After the spectra at 15 K are taken, the sample is heated at a rate of 25 K h^{-1} until it is completely desorbed from the substrate. During the heating of the sample, spectra are continuously recorded to obtain spectra for different temperature settings. Consequently, an ice spectrum recorded for a specific temperature, actually covers a temperature range of ±0.8 K from the central value. This is also the reason why spectra are recorded at 0.5 cm^{-1} resolution, as this is an optimum between spectral resolution and time needed to perform a full scan; with increasing scan time the uncertainty of the ice temperature would increase. Apart from temperatures close to a phase transition or desorption temperature, this does not cause any inaccuracies. More experimental details can be found in (Terwisscha van Scheltinga et al. 2018).

2.1. Ice samples

Astronomical observations supported by laboratory studies have shown that the molecular constituents of interstellar ices are partially structured in layers rather than homogeneously mixed. Dust grains are initially covered by layers of water, due to surface reactions of H atoms and O atoms and direct freeze-out of gas-phase H_2O (Cuppen et al. 2010; Linnartz et al. 2015). During this stage CO_2 and CH_4 are also formed (Öberg et al. 2008; Ioppolo et al. 2011; Qasim et al. 2020). As the density increases and temperatures further drop, CO starts to accrete rapidly. Subsequent hydrogenation of CO ultimately results in methanol formation within a CO rich ice (Boogert et al. 2015; Linnartz et al. 2015). In an attempt to simulate the infrared spectra of acetone in these different ice layers, the mixtures prepared in this work contain acetone mixed with some of the more abundant interstellar ice components: H_2O, CO_2, CO, CH_4, and CH_3OH. Additionally, acetone is mixed in H_2O:CO_2, H_2O:CH_4, and CO:CH_3OH mixtures. The mixtures are prepared with acetone ratios of 1:5 (i.e., 1 molecule of acetone for 5 matrix molecules) and 1:20. These ratios are relatively high compared to COMs (likely to have been) identified in astronomical data but are expected to provide representative spectra. Table 1 shows the composition and mixing ratios of all ice samples studied in this work. For all the investigated ice samples, spectra are collected between 15 K and 200 K. In this work, the spectra are analyzed until thermal desorption of the major matrix components ($T \sim 30$ K for CO, $T \sim 100$ K for CO_2, $T \sim 140$ K for the CH_3OH-containing ices and $T \sim 160$ K for the H_2O-containing ices) or until the acetone bands are no longer detectable.

2.2. Analysis protocol

All the spectra are baseline-corrected using *Origin* and the acetone bands are identified by comparison with the results presented by Hudson et al. (2018). From the acetone infrared features visible in the pure ice spectra, the strongest ones ($A > 10^{-18}$, see Hudson et al. 2018) are selected. From these, only

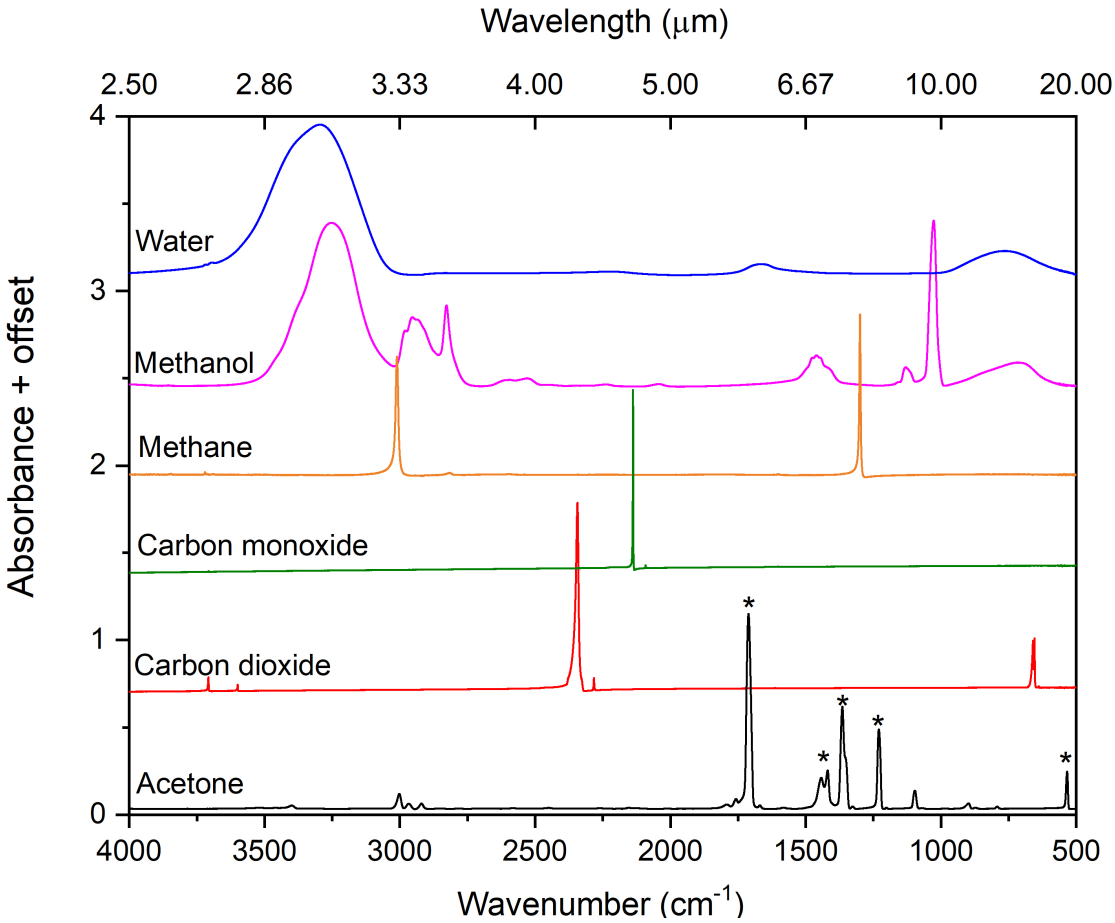

Fig. 1. Infrared ice spectra of pure CH_3COCH_3 (black), CO_2 (red), CO (green), CH_4 (orange), CH_3OH (magenta) and H_2O (blue). The acetone absorption bands marked with an asterisk have been selected for an in-depth study as most suited acetone tracers for future JWST surveys.

the transitions that have no obvious spectral overlap with bands originating from other abundant ice species are characterized (i.e., peak position and FWHM) using a personal *Matlab* script. Figure 1 shows the infrared spectrum of pure CH_3COCH_3 ice (bottom) and the spectra of the other ice components that are used in the analyzed samples: H_2O, CH_3OH, CH_4, CO_2, and CO. The five selected acetone bands analyzed in this work are marked in Fig. 1 with an asterisk. These bands are: the CO in-plane deformation band around 533 cm^{-1} (18.8 μm); the CCC asymmetric stretch band around 1228 cm^{-1} (8.14 μm); the CH_3 symmetric deformation band around 1363 cm^{-1} (7.34 μm); the CH_3 asymmetric deformation band around 1418 cm^{-1} (7.05 μm); and the C=O stretch band around 1710 cm^{-1} (5.85 μm), see Table 2.

The band strength (A) of a vibrational mode can be used to calculate the number of absorbing species that count for an absorption feature. Once known, it can be used to derive the column density for a specific molecule from an infrared spectrum. Physically, the integrated absorbance of a vibrational mode is related to the changes in the electron charge distribution upon excitation. Since the electronic configuration of a molecule changes due to the interaction with the surrounding species, the band strength depends on the composition and morphology of the ice. In order to better derive abundances or upper limits of molecules in astronomical data, it is advantageous to know the band strength of COMs when embedded in ices with compositions similar to those in which such molecules are expected to be found in. In this work, we derive the apparent band strength (A') of the acetone vibrational modes, when acetone is embedded in different ice matrices. These values of the apparent band strength relative to the values reported by Hudson et al. (2018) are displayed in Appendix A. The estimated errors in this procedure are around 20%.

3. Results and discussion

This section presents a series of representative spectra. All other spectra are shown in Figs. A.1 to A.16 in the Appendix. These spectra not only allow to search for acetone ice features, but the differences that become clear when comparing the data for different settings, also offer a diagnostic tool for further ice characterization.

Figures 2 through 5 show the C=O stretching and the CCC asymmetric stretching of acetone for temperatures ranging from 15 K to 160 K, in pure ice and in mixtures with an acetone ratio of 1:5. For improved visualization, the spectra at different temperatures are offset and it should be noted that the panel showing acetone in pure form (left panel in all figures) is displayed at a different scale compared to the panels presenting the ice mixture spectra. These and all other spectra shown in Appendix A are available in full from the Leiden Ice Database[2]. A compilation of all acetone features at different temperatures can be found in Appendix B. The integrated absorbance of the selected acetone bands is available from Appendix C. Spectra recorded at intermediate temperatures and not listed here are available upon request.

[2] https://icedb.strw.leidenuniv.nl/

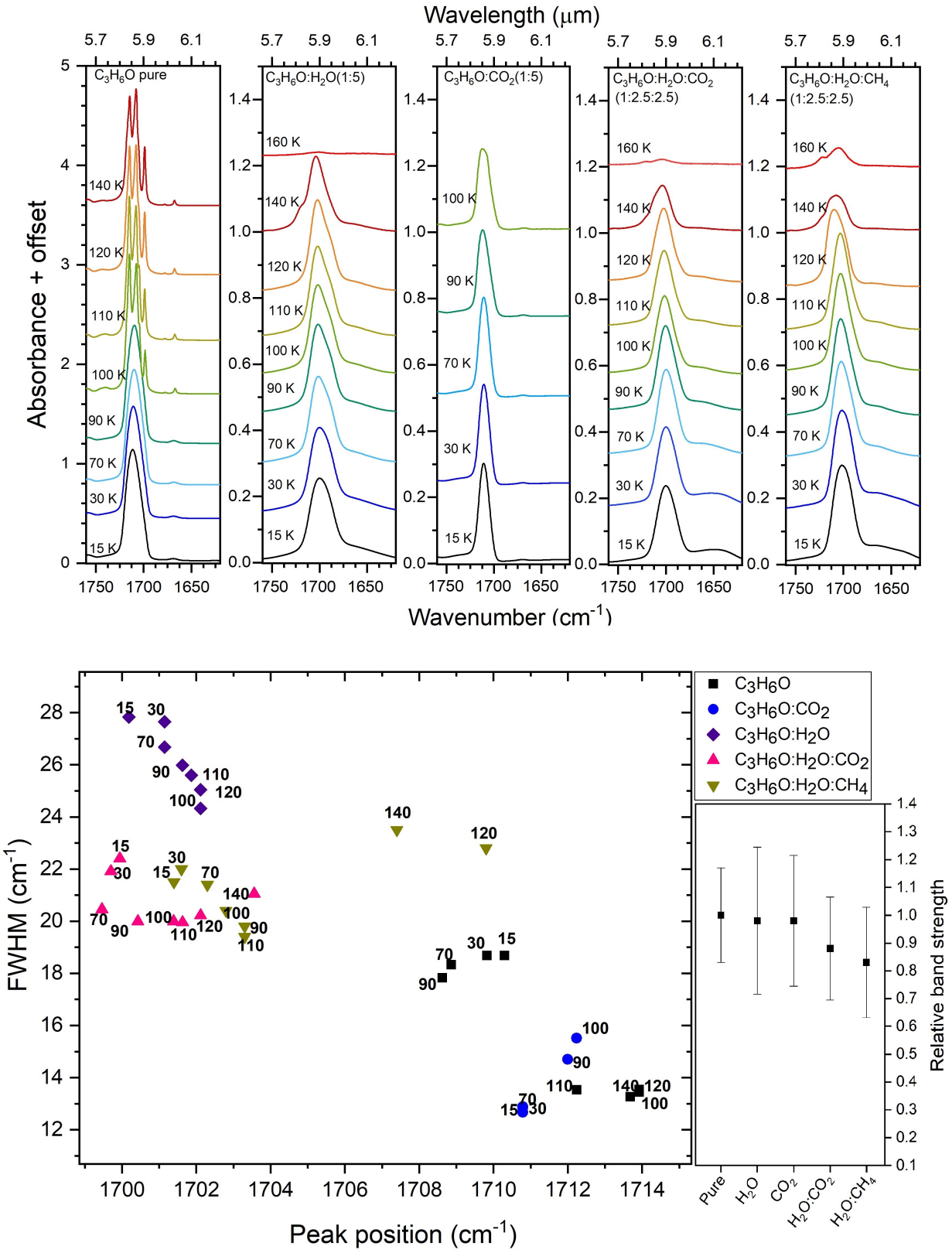

Fig. 2. *Upper panel*: infrared spectra in the range of 1760–1630 cm^{-1} (5.68–6.13 μm) showing the C=O stretch band of acetone embedded in different ice mixtures, *from left to right*: pure CH_3COCH_3, CH_3COCH_3:H_2O(1:5), CH_3COCH_3:CO_2(1:5), CH_3COCH_3:H_2O:CO_2(1:2.5:2.5), and CH_3COCH_3:H_2O:CH_4(1:2.5:2.5). The spectra at different temperatures are offset for improved visualization. *Bottom left*: peak position vs. FWHM plot for the C=O stretch band in different ice matrices, represented by the different colors, and for different temperatures, indicated by the numbers in the graph. *Bottom right*: apparent band strength for the acetone C=O stretch band at 15 K in the various matrices divided by the band strength for pure acetone from Hudson et al. (2018).

Table 2. Peak positions and band strengths of the pure acetone ice bands studied in this work.

Vibrational mode	Peak position (cm^{-1})		A' [(b)]
	15 K [(a)]	10 K [(b)]	(10^{-18} cm mol^{-1})
CO in plane deformation	532.7	533.6	2.13
CCC asymmetric stretch	1228.4	1228.9	7.35
CH_3 symmetric deformation	1363.4	1364.4	13.9
CH_3 asymmetric deformation	1417.9	1418.9	9.19
C=O stretching	1710.3	1711.4	26.7

Notes. The acetone band position and strengths for the amorphous ice at 10 K (Hudson et al. 2018) are shown for comparison.
References. [(a)]This work. [(b)]Hudson et al. (2018).

3.1. Pure acetone ice

Table 2 lists the infrared bands of acetone that have been selected as the best-suited tracers of acetone ice in space. As expected, the peak position values for pure acetone ice are close to those reported by Hudson et al. (2018) for amorphous acetone ice at 10 K. The pure acetone ice remains amorphous between 15 K and 90 K and there are no significant changes seen in the peak positions and band shapes. At 93 K, there is an abrupt sharpening of all the investigated bands, characteristic for the transition to crystalline acetone. The peak positions of the acetone bands also change after crystallization. From 100 K up to 140 K, the bandwidths show no appreciable changes. When the pure acetone ice is heated to temperatures above 140 K, the intensity of the acetone bands starts decreasing and drops below the detection sensitivity of our IR technique when the sample reaches 148 K. This temperature is close to the value presented by Hudson et al. (2018), who reported that acetone thermally desorbs around 150 K.

3.2. Peak positions of acetone features in ice mixtures

The C=O stretch vibrational mode, around 1710 cm^{-1} (5.85 μm), is the strongest acetone band ($A = 2.67 \times 10^{-17}$ cm molecule^{-1}). The resulting bands in different matrix environments and as function of temperature are shown in Figs. 2 and 3 for the low dilution mixtures (1:5) and in Figs. A.7 and A.8 for the high dilution mixtures (1:20). This mode is partially superimposed on the OH bending mode of water as well as other molecules detected in astrophysical ices, such as the N–H bending mode of ammonia (Bouilloud et al. 2015; Boogert et al. 2015). However, since this mode is strong, it is easily identified even in the diluted mixtures (see Figs. A.7 and A.8). In H_2O, CO_2, and CO matrices, at low temperatures, this vibrational mode is present as a single feature while in CH_3OH-containing ices, it appears as a two-component feature, which is likely due to the formation of binary complexes with methanol (Han & Kim 1996).

A point worth stressing is that multi-component peaks, such as the ones showing up with an increase in temperature or when acetone is embedded in certain ice matrices, are usually associated with the vibrational modes of interacting molecules within the ice structure. In methanol-acetone ices, the formation of acetone dimers, trimers, and tetramers induces the appearance of specific absorption bands (Kollipost et al. 2015). When the sample is warmed, molecules are reoriented inside the ice structure, adopting the most energetically favourable configurations, that is, some arrangement of molecules are more likely than others. The intensity of the peaks associated with these dominant configurations at a specific temperature appears enhanced in the spectra. Unfortunately, contrary to the gas phase, little is known about the exact orientations of molecules in amorphous ices, an issue that is even more significant in the case of mixed ices. The data presented here reflect these processes and will prove helpful in identifying COMs in interstellar ices, however, the specific explanation of the spectroscopic behaviour is outside the scope of this work. We refer to Zhang et al. (1993), Han & Kim (1996), Kollipost et al. (2015), where the assignment of some of the multi-component infrared bands of acetone in different solid and liquid matrices has been investigated.

The shape and FWHM of the acetone bands in the H_2O-containing mixtures are very similar. In the CH_3COCH_3:H_2O:CO_2 and CH_3COCH_3:H_2O:CH_4 ices, the analyzed bands exhibit similar shifts, broadening, and splitting patterns. For example, the peak positions for the acetone bands in these mixtures usually vary less than 2 cm^{-1} at 15 K for ices with the same acetone ratio (see Appendix B). In these H_2O-rich ices, the C=O stretch appears as a broad feature, shifted towards lower frequencies with respect to the pure acetone ice. The largest shifts towards lower frequencies are observed for the CH_3COCH_3:H_2O:CO_2 ices: 1699.9 cm^{-1} (5.88 μm) and 1695.6 cm^{-1} (5.90 μm) for the samples at 1:5 and 1:20 dilution ratios, respectively, and for the CH_3COCH_3:H_2O:CH_4(1:10:10) ice, where this mode appears at 1697.5 cm^{-1}. In the CO matrix, this band exhibits the largest shifts towards higher wavenumbers, and is found at 1715.9 cm^{-1} (5.83 μm) and 1717.3 cm^{-1} (5.82 μm) for the 1:5 and 1:20 ratios, respectively. By warming the ices to temperatures higher than 120 K, the carbonyl band mode sharpens and appears as a three-component feature in the CH_3OH-containing ices, similar to the pure acetone ice. In all these H_2O-containing ices, the peak sharpening and splitting are not observed, while in the CH_3COCH_3:CO and CH_3COCH_3:CO_2 ices, the matrix is mostly desorbed before 120 K is reached (see Fig. 3).

The data collected in this work show that the C=O stretch peak position of acetone varies significantly, depending on the ice matrix and temperature. In the studied 15 K ices, the acetone carbonyl stretching mode is between 1695 and 1717 cm^{-1} (5.90–5.82 μm). These peak shifts occur due to matrix effects, which add further diagnostic value, and should be taken into account when trying to assign peaks in astronomical spectra.

The CH_3 asymmetric deformation mode of acetone, around 1418 cm^{-1} (7.05 μm), overlaps with the CH_3 bending modes of methanol (Bouilloud et al. 2015). All resulting spectra are shown in Figs. A.1 and A.2 (low dilution) and Figs. A.9 and A.10

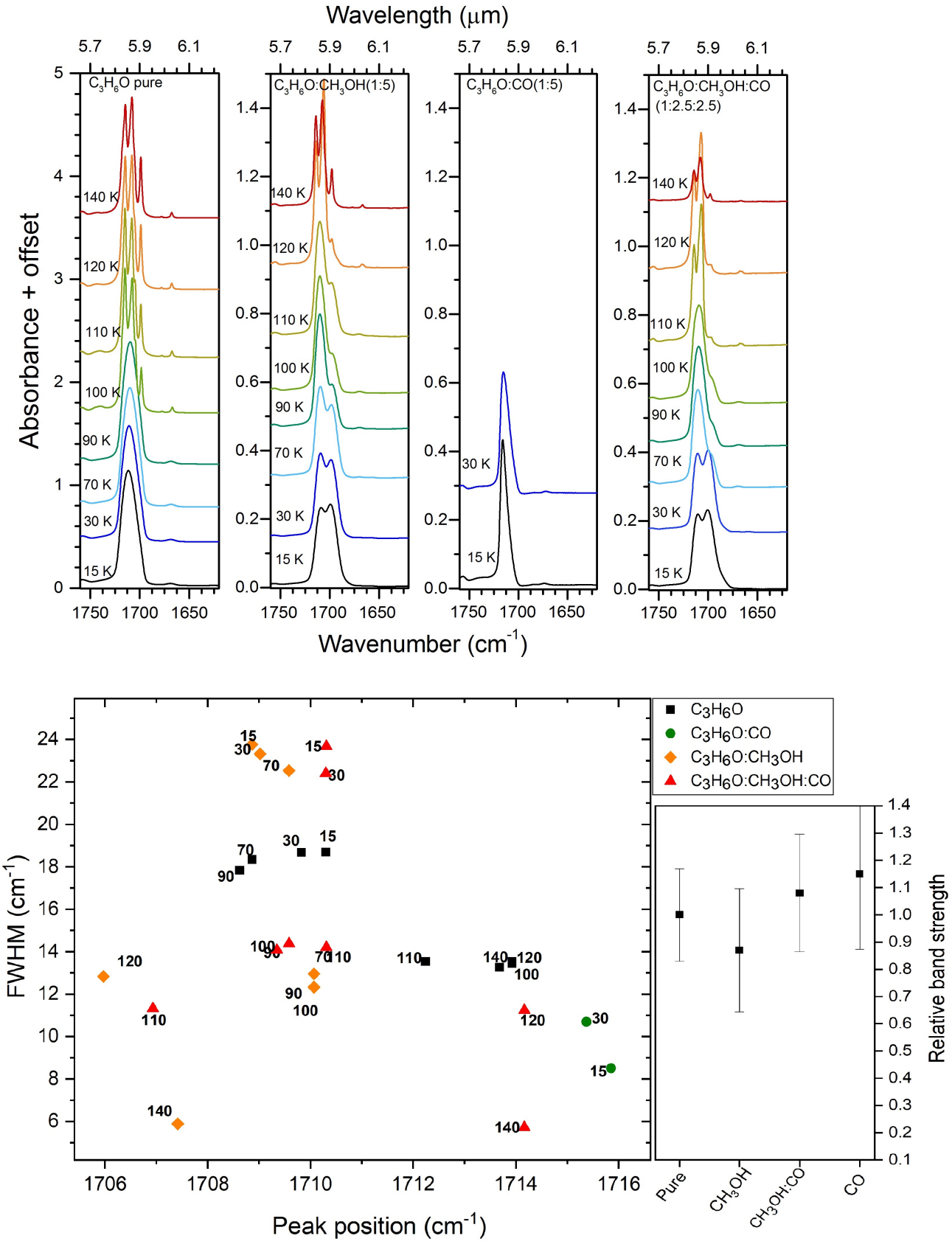

Fig. 3. *Upper panel*: infrared spectra in the range of 1760–1630 cm^{-1} (5.68–6.13 μm) showing the C=O stretch band of acetone embedded in different ice mixtures, *from left to right*: pure CH_3COCH_3, CH_3COCH_3:CH_3OH(1:5), CH_3COCH_3:CO(1:5), and CH_3COCH_3:CH_3OH:CO(1:2.5:2.5). The spectra at different temperatures are offset for improved visualization. *Bottom left*: peak position vs. FWHM plot for the C=O stretch band in different ice matrices, represented by the different colors, and for different temperatures, indicated by the numbers in the graph. *Bottom right*: apparent band strength for the acetone C=O stretch band at 15 K in the various matrices divided by the band strength for pure acetone from Hudson et al. (2018).

(high dilution). At temperatures higher than 100 K, this band narrows, but still overlaps with the CH_3OH bands (Figs. A.2 and A.10). This makes the detection of this feature in astronomical data very unlikely when CH_3OH is present, especially at low temperatures when the bands are broader.

The CH_3 symmetric deformation mode of acetone, between 1380 and 1335 cm^{-1} (7.25–7.49 μm), however, can be relatively easily identified. The corresponding spectra are shown in Figs. A.3 and A.4 (1:5 mixtures) and Figs. A.11 and A.12 (1:20 mixtures). This vibrational mode appears as a two-component feature or as a feature with a shoulder in all spectra. For pure acetone ice and the CH_3OH-containing ices, the shoulder at lower wavenumbers (around 1352 cm^{-1}) narrows when the crystallization of acetone-methanol matrix takes place, revealing that it is in fact composed of two other components, which are around 1349.2 cm^{-1} and 1361.3 cm^{-1} (Figs. A.4 and A.12). For the pure ice, these features appear at 100 K, and for the CH_3OH-bearing ices (ratio 1:5) these features appear at temperatures higher than 120 K. For the CH_3COCH_3:CO:CH_3OH(1:10:10) ice, the splitting of the CH_3 asymmetric deformation mode is also observed at high temperatures. In the CH_3COCH_3:CO_2 mixtures a weak feature, close to 1380 cm^{-1} (7.24 μm), is observed. This feature disappears at temperatures higher than 90 K.

The CCC asymmetric stretch band of acetone, around 1230 cm^{-1} (8.1 μm) holds much potential as a tracer of acetone in interstellar ices (see Figs. 4 and 5 for the spectra of 1:5 mixtures and Figs. A.13 and A.14 for the spectra of 1:20 mixtures). The 1230 cm^{-1} band does not overlap with bands of the matrix components studied in this work. This feature is also one of the few bands of acetone that does not overlap with the infrared bands of acetaldehyde (CH_3CHO) (Terwisscha van Scheltinga et al. 2018), a possible precursor of solid acetone in interstellar ices (Garrod et al. 2008). In CO and CO_2 matrices this band appears at wavenumbers closer to the value of pure acetone (1228.4 cm^{-1}). In H_2O-containing ices, this feature is shifted to higher wavenumbers: between 1240 and 1245 cm^{-1}. In the CH_3OH-containing ices, this band appears as a two-component feature at 15 K, at 1226.0 cm^{-1} and 1238.1 cm^{-1} for the 1:5 mixture, and 1225.5 cm^{-1} and 1238.1 cm^{-1} for the 1:20 mixture.

The CCC asymmetric stretch band is composed of two components that become visible upon narrowing, when the ice is heated to temperatures higher than 100 K. In the pure acetone ice and in the methanol-containing mixtures, the component at higher wavenumber increases in strength with respect to the component at lower wavenumber, when warming the ices at temperatures higher than 100 K and 110 K, for the pure ice and the methanol-containing mixtures, respectively. In water-rich matrices the CCC asymmetric stretch band of acetone appears as a broad feature. As the sample is heated, the peak at low wavenumbers increases in intensity compared to the peak at high wavenumbers, the opposite of what is observed for the methanol-containing mixtures. In this way, the difference in the intensity between the two peaks that compose the CCC asymmetric stretch band may add further insights about the composition of the ice. In ices where CH_3OH is an abundant component, the different intensities of the peaks composing the CCC asymmetric stretch band can be related to the ice temperature.

In pure acetone ices, the CO in-plane deformation mode gives rise to a band at 532.7 cm^{-1} (18.77 μm). Figures A.5 and A.6 (1:5 mixtures) and Figs. A.15 and A.16 (1:20 mixtures) show the CO in-plane deformation band in the spectra recorded for different matrix environments. The position of this band is highly affected by the presence of CO_2 and H_2O, and shifts to higher wavenumbers: 535.6 cm^{-1} (18.67 μm) and 547.0 cm^{-1} (18.28 μm) for CO_2 and H_2O, respectively. This effect is more pronounced in the 1:20 mixtures, where this mode is located at 536.1 cm^{-1}. This trend is probably related to the fact that acetone can interact as an electron donor in the presence of a Lewis acid, as observed by Cha et al. (1999). The profile of the CO deformation mode makes this band a good acetone tracer candidate when acetone is in a water-poor environment, since in the CH_3COCH_3:H_2O(1:20) ice, this band is hard to detect.

3.3. FWHM of acetone bands in ice mixtures

In all the H_2O-containing ice samples, the acetone peaks remain broad until 140 K, because the water matrix prohibits the acetone to crystallize. From this temperature onwards, a decrease in the intensity of the acetone peaks is observed, indicating that acetone starts to desorb. In the CH_3OH containing ices, the sharpening and splitting of the acetone bands are observed when reaching temperatures between 110 K and 120 K. The band sharpening and splitting may be due to a delayed crystallization of acetone. It is also possible that a thermal induced re-orientation of molecules creates a more organized environment for the acetone molecules and breaks some hydrogen bonds between methanol and acetone, making the peaks become sharper. The acetone desorption in these samples happens gradually in the range between 140 K and 150 K.

The CO and CO_2-containing ice mixtures were analyzed until their desorption temperature. When this temperature is reached, a decrease in the acetone peak intensity is observed along with matrix desorption. This decrease may be associated with co-desorption, making the quantitative analysis of the intensity of acetone peaks not ideal. However, other findings can be reported about the shape of the acetone peaks in the remaining ice that may be useful. In the CH_3COCH_3:CO ices, all the acetone features are sharper than in the pure acetone ice at 15 K (see Appendix B). From 20 K, the FWHM of the peaks starts to increase. The C=O stretch mode, for example, broadens from 8.5 cm^{-1} at 15 K to 10.7 cm^{-1} at 30 K in the CH_3COCH_3:CO(1:5) mixture and from 6.8 cm^{-1} at 15 K to 9.7 cm^{-1} at 30 K in the CH_3COCH_3:CO(1:20) mixture. When heating the remaining ice to temperatures above 88 K, the acetone bands become sharper, indicating the onset of acetone crystallization. The (1:5) mixture is the only sample for which characteristic crystalline acetone peaks are observed at temperatures lower than 90 K. In the (1:20) mixture, the crystallization of the remaining acetone ice is found around 97 K. In the CH_3COCH_3:CO_2 samples, the CO_2 desorption occurs between 90 K and 100 K. The presence of abundant CO_2 in the sample at temperatures between 90 K and 100 K makes that the crystalline features of acetone appear at temperatures between 101 K and 105 K.

4. Conclusions

The knowledge of the composition of ices outside of the Solar System may drastically change with the upcoming JWST observations. In order to identify features of frozen COMs in the astronomical data, laboratory infrared spectra are necessary for comparison. This work provides an extensive collection of infrared spectra of acetone (CH_3COCH_3) in astronomically relevant ice mixtures, at temperatures ranging from 10 K up to 160 K. The strongest acetone bands are characterized in terms of peak position, FWHM, and band intensity ratios. The

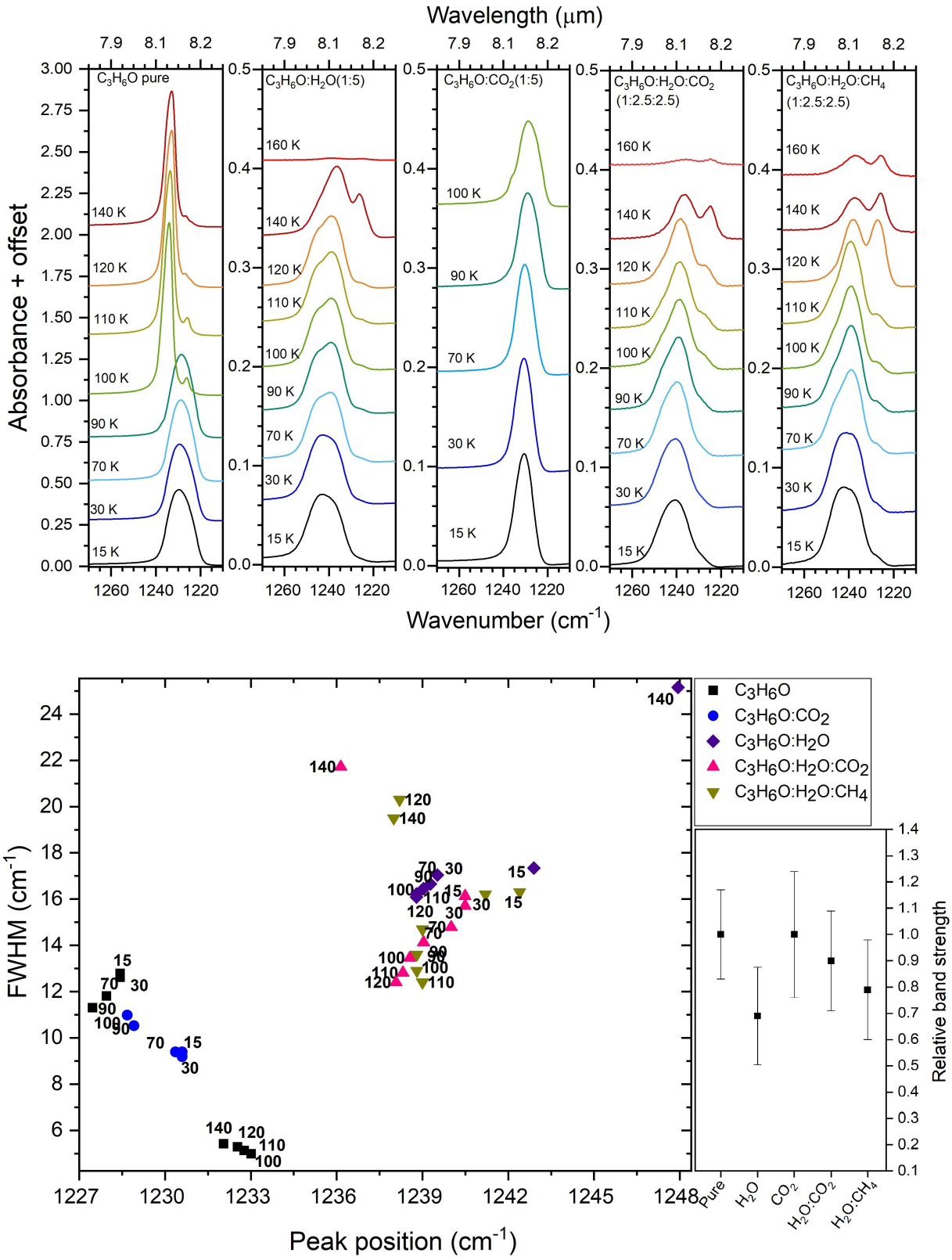

Fig. 4. *Upper panel*: infrared spectra in the range of 1270–1210 cm^{-1} (7.87–8.26 μm) showing the CCC asymmetric stretch band of acetone in different ice mixtures, *from left to right*: pure CH_3COCH_3, CH_3COCH_3:H_2O(1:5), CH_3COCH_3:CO_2(1:5), CH_3COCH_3:H_2O:CO_2(1:2.5:2.5), and CH_3COCH_3:H_2O:CH_4(1:2.5:2.5). The spectra at different temperatures are offset for improved visualization. *Bottom left*: peak position vs. FWHM plot for the CCC asymmetric stretch band in different ice matrices, represented by the different colors, and for different temperatures, indicated by the numbers in the graph. *Bottom right*: apparent band strength for the acetone CCC asymmetric stretch band at 15 K in the various matrices divided by the band strength for pure acetone from Hudson et al. (2018).

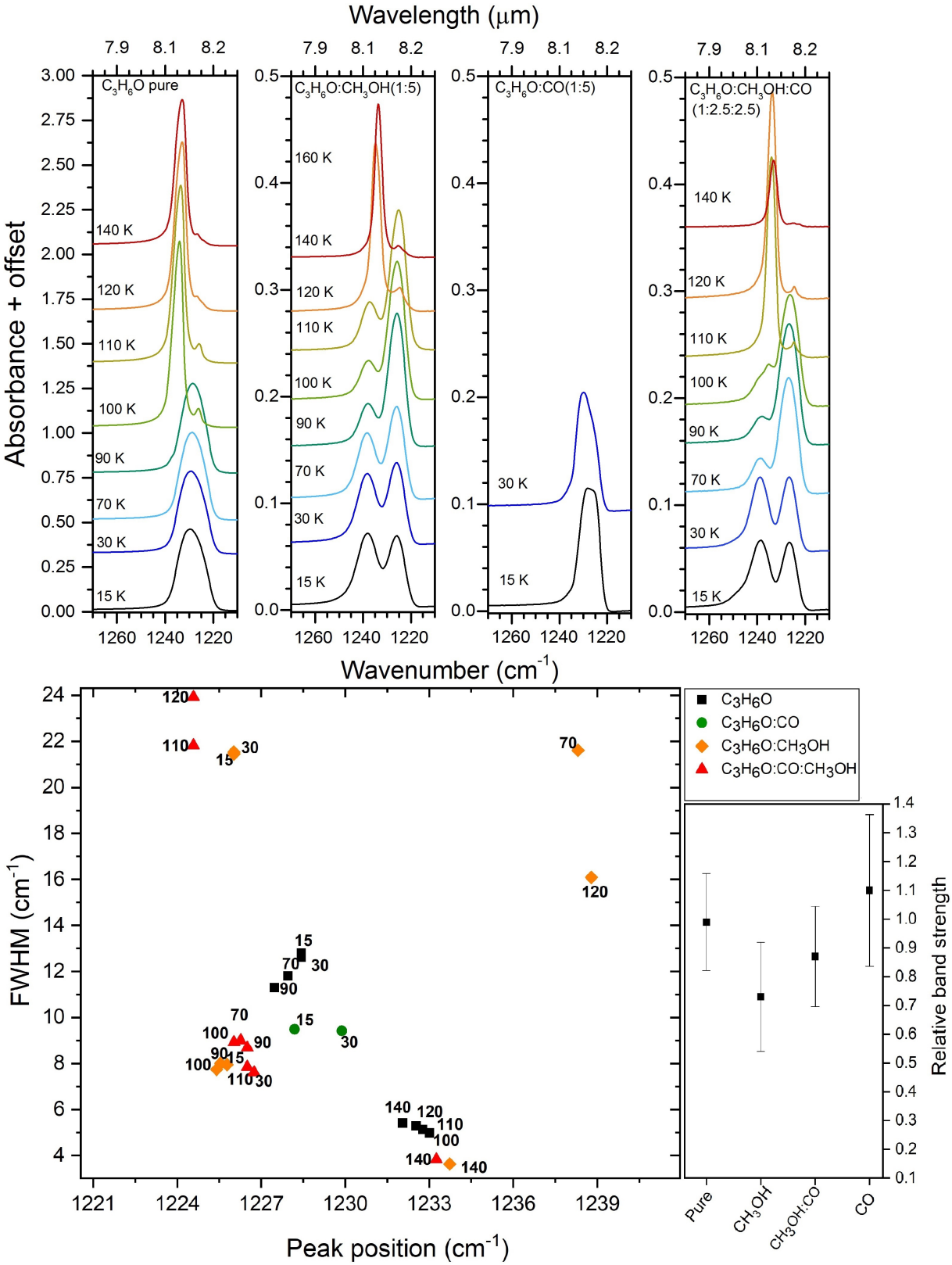

Fig. 5. *Upper panel*: infrared spectra in the range of 1270–1210 cm^{-1} (7.87–8.26 μm) showing the CCC asymmetric stretch band of acetone in different ice mixtures, *from left to right*: pure CH_3COCH_3, CH_3COCH_3:CH_3OH(1:5), CH_3COCH_3:CO(1:5), and CH_3COCH_3:CH_3OH:CO(1:2.5:2.5). The spectra at different temperatures are offset for improved visualization. *Bottom left*: peak position vs. FWHM plot for the CCC asymmetric stretch band in different ice matrices, represented by the different colors, and for different temperatures, indicated by the numbers in the graph. *Bottom right*: apparent band strength for the acetone CCC asymmetric stretch band at 15 K in the various matrices divided by the band strength for pure acetone from Hudson et al. (2018).

bands that are most promising for detection of solid acetone in astronomical data are the CCC asymmetric stretch band around 1228 cm^{-1} (8.14 μm), the CH_3 symmetric deformation band around 1363 cm^{-1} (7.34 μm) and the C=O stretch band, around 1710 cm^{-1} (5.85 μm). Other conclusions are summarized below:

1. The acetone C=O stretch band is found in the range of 1715.9–1695.6 cm^{-1} (5.83–5.90 μm) for the analyzed acetone-containing ice mixtures. This mode shifts towards higher wavenumbers in the CO and CO_2 containing mixtures and to lower wavenumbers in the H_2O-rich mixtures.
2. The CH_3 symmetric stretch is found in the range of 1353–1373 cm^{-1} (7.28–7.39 μm). This band is present as a two component feature in H_2O, CO_2, CO, H_2O:CO_2 and H_2O:CH_4 ice matrices. The two components become less discernible in the CH_3OH containing ices.
3. The CCC asymmetric stretch is found in the range of 1224–1245 cm^{-1} and shifts towards higher wavenumbers in the H_2O-containing samples. This band is composed of two components and the different intensities of the two components offer a tool for determining the temperature of interstellar ices and for further determining their composition.

Acknowledgements. This work has been made possible through financial support by NOVA, the Netherlands Research School for Astronomy. We thank Dr. Melissa McClure and Dr. Adwin Boogert for many stimulating discussions.

References

Berné, O., Mulas, G., & Joblin, C. 2013, A&A, 550, L4
Boogert, A. A., Gerakines, P. A., & Whittet, D. C. 2015, ARA&A, 53, 541
Bossa, J.-B., Isokoski, K., de Valois, M., & Linnartz, H. 2012, A&A, 545, A82
Bouilloud, M., Fray, N., Bénilan, Y., et al. 2015, MNRAS, 451, 2145
Cami, J., Bernard-Salas, J., Peeters, E., & Malek, S. E. 2010, Science, 329, 1180
Campbell, E. K., Holz, M., Gerlich, D., & Maier, J. P. 2015, Nature, 523, 322
Cha, D. K., Kloss, A. A., Tikanen, A. C., & Fawcett, W. R. 1999, Phys. Chem. Chem. Phys., 1, 4785
Combes, F., Gerin, M., Wootten, A., et al. 1987, A&A, 180, L13
Cordiner, M., Linnartz, H., Cox, N., et al. 2019, ApJ, 875, L28
Cuppen, H., Ioppolo, S., Romanzin, C., & Linnartz, H. 2010, Phys. Chem. Chem. Phys., 12, 12077
Dawes, A., Mukerji, R. J., Davis, M. P., et al. 2007, J. Chem. Phys., 126, 244711
Duarte, E. S., Domaracka, A., Boduch, P., et al. 2010, A&A, 512, A71
Ehrenfreund, P., & Charnley, S. B. 2000, ARA&A, 38, 427
Fedoseev, G., Cuppen, H. M., Ioppolo, S., Lamberts, T., & Linnartz, H. 2015, MNRAS, 448, 1288
Friedel, D., & Snyder, L. 2008, ApJ, 672, 962
Friedel, D. N., Snyder, L., Remijan, A. J., & Turner, B. 2005, ApJ, 632, L95
Fuente, A., Cernicharo, J., Caselli, P., et al. 2014, A&A, 568, A65
Garrod, R. T., Weaver, S. L. W., & Herbst, E. 2008, ApJ, 682, 283
Gerakines, P., Schutte, W., & Ehrenfreund, P. 1996, A&A, 312, 289
Gibb, E., Whittet, D., Boogert, A., & Tielens, A. 2004, ApJS, 151, 35
Han, S. W., & Kim, K. 1996, J. Phys. Chem., 100, 17124
Herbst, E., & Van Dishoeck, E. F. 2009, ARA&A, 47, 427
Herbst, E., Giles, K., & Smith, D. 1990, ApJ, 358, 468
Hudson, R., & Moore, M. 1999, Icarus, 140, 451
Hudson, R., & Moore, M. 2001, J. Geophys. Res.: Planets, 106, 33275
Hudson, R. L., Gerakines, P. A., & Ferrante, R. F. 2018, Spectrochim. Acta Part A: Mol. Biomol. Spectrosc., 193, 33
Ioppolo, S., Van Boheemen, Y., Cuppen, H., van Dishoeck, E. F., & Linnartz, H. 2011, MNRAS, 413, 2281
Isokoski, K., Bossa, J.-B., Triemstra, T., & Linnartz, H. 2014, Phys. Chem. Chem. Phys., 16, 3456
Kaiser, R. I., Maity, S., & Jones, B. M. 2014, Phys. Chem. Chem. Phys., 16, 3399
Kollipost, F., Domanskaya, A. V., & Suhm, M. A. 2015, J. Phys. Chem. A, 119, 2225
Lee, J.-E., Lee, S., Baek, G., et al. 2019, Nat. Astron., 3, 314
Linnartz, H., Ioppolo, S., & Fedoseev, G. 2015, Int. Rev. Phys. Chem., 34, 205
Lykke, J. M., Coutens, A., Jørgensen, J. K., et al. 2017, A&A, 597, A53
McGuire, B. A. 2018, ApJS, 239, 17
Öberg, K. I. 2016, Chem. Rev., 116, 9631
Öberg, K. I., Fraser, H. J., Boogert, A. A., et al. 2007, A&A, 462, 1187
Öberg, K. I., Boogert, A. A., Pontoppidan, K. M., et al. 2008, ApJ, 678, 1032
Öberg, K. I., Garrod, R. T., van Dishoeck, E. F., & Linnartz, H. 2009, A&A, 504, 891
Öberg, K. I., Boogert, A. A., Pontoppidan, K. M., et al. 2011, ApJ, 740, 109
Palumbo, M. E. 2005, Journal of Physics: Conference Series (IOP Publishing), 6, 211
Qasim, D., Fedoseev, G., Chuang, K.-J., et al. 2020, Nat. Astron., https://doi.org/10.1038/s41550-020-1054-y
Sellgren, K., Werner, M. W., Ingalls, J. G., et al. 2010, ApJ, 722, L54
Snyder, L. E., Lovas, F. J., Mehringer, D. M., et al. 2002, ApJ, 578, 245
Terwisscha van Scheltinga, J., Ligterink, N., Boogert, A., van Dishoeck, E., & Linnartz, H. 2018, A&A, 611, A35
Watanabe, N., & Kouchi, A. 2002, ApJ, 571, L173
Zhang, X. K., Lewars, E. G., March, R. E., & Parnis, J. M. 1993, J. Phys. Chem., 97, 4320
Zou, L., & Weaver, S. L. W. 2017, ApJ, 849, 139

Appendix A: IR spectra and apparent band strengths

In this section, the infrared spectra of the selected vibrational modes of acetone (see Table 2) are given, for pure acetone and for acetone in different ice mixtures (upper panels). The peak position versus FWHM for the investigated bands for the different ices is displayed in the bottom left panel of each figure. The corresponding values are listed in the tables in Appendix B. The relative apparent band strengths of these bands (in relation to the values for pure acetone ice at 10 K reported by Hudson et al. 2018) are displayed in the bottom right panel for the different mixtures studied here (Figs. A.1–A.16).

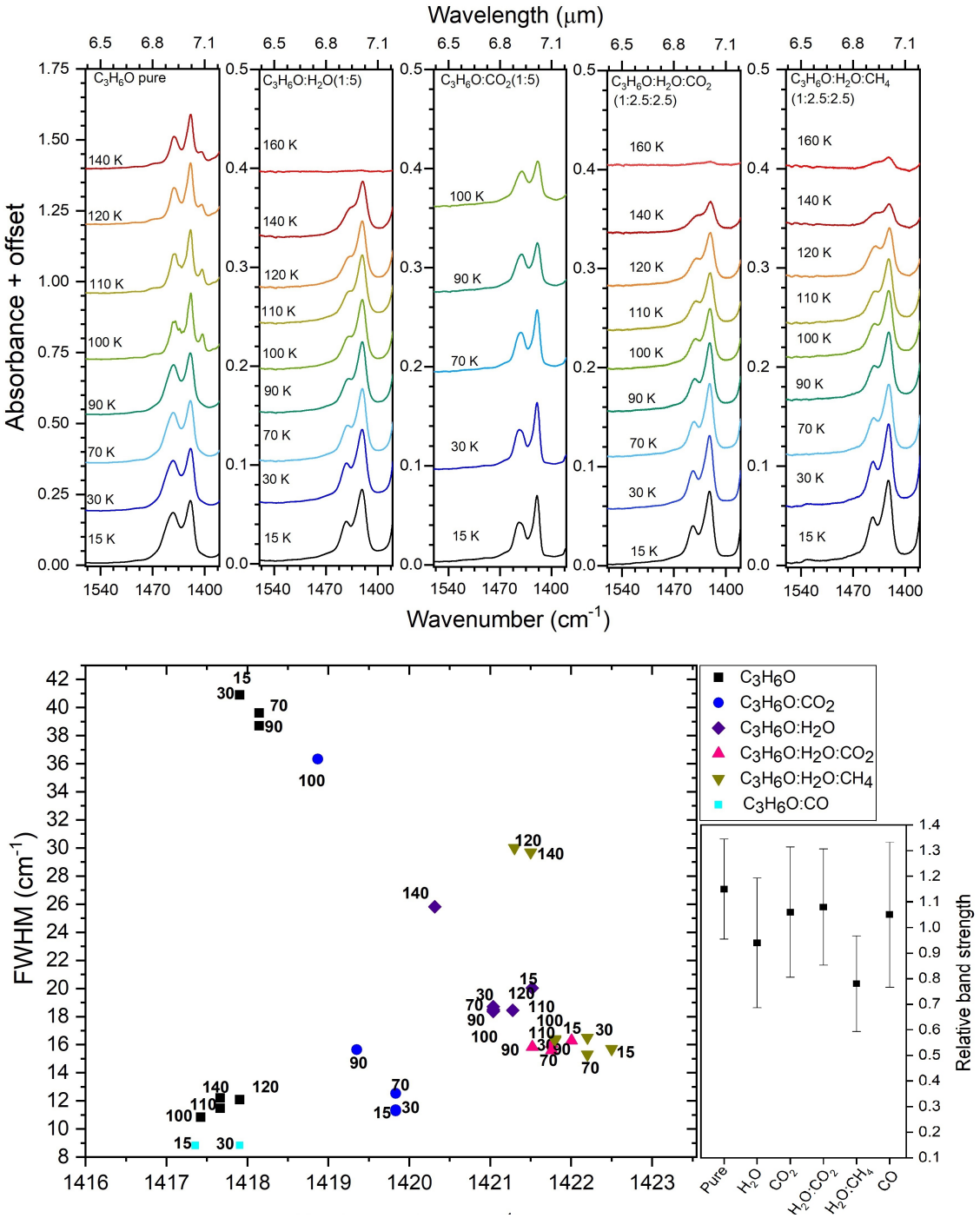

Fig. A.1. *Upper panel*: infrared spectra in the range of 1550–1390 cm^{-1} (6.45–7.19 μm) showing the CH_3 asymmetric deformation band of acetone embedded in different ice mixtures, *from left to right*: pure CH_3COCH_3, CH_3COCH_3:H_2O(1:5), CH_3COCH_3:CO_2(1:5), CH_3COCH_3:H_2O:CO_2(1:2.5:2.5), and CH_3COCH_3:H_2O:CH_4(1:2.5:2.5). The spectra at different temperatures are offset for improved visualization. *Bottom left*: peak position vs. FWHM plot for the CH_3 asymmetric deformation band in different ice matrices, represented by the different colors, and for different temperatures, indicated by the numbers in the graph. *Bottom right*: apparent band strength for the acetone CH_3 asymmetric deformation band at 15 K in the various matrices with respect to the band strength for pure acetone from Hudson et al. (2018).

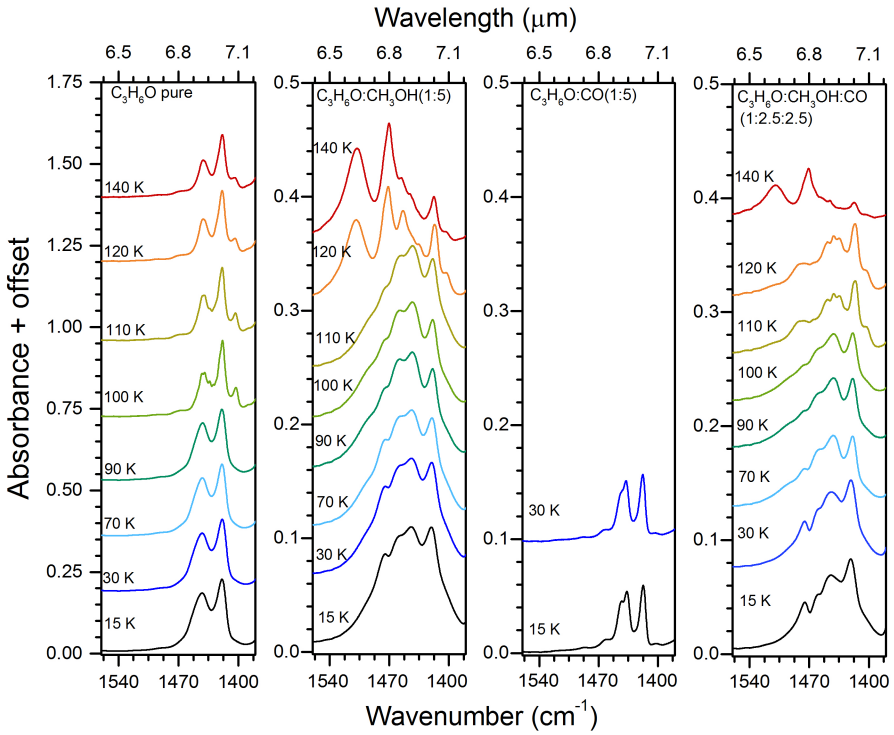

Fig. A.2. Infrared spectra in the range of 1550–1390 cm^{-1} (6.45–7.19 μm) showing the CH_3 asymmetric deformation band of acetone embedded in different ice mixtures, *from left to right*: pure CH_3COCH_3, CH_3COCH_3:CH_3OH(1:5), CH_3COCH_3:CO(1:5), and CH_3COCH_3:CH_3OH:CO(1:2.5:2.5). The spectra at different temperatures are offset for improved visualization. Since the FWHM of the CH_3 asymmetric deformation band was not measured in the methanol-containing mixtures (due to the overlap with the methanol CH_3 bending mode), the peak position vs. FWHM plot for this acetone feature in CO matrix is displayed with the data in Fig. A.1.

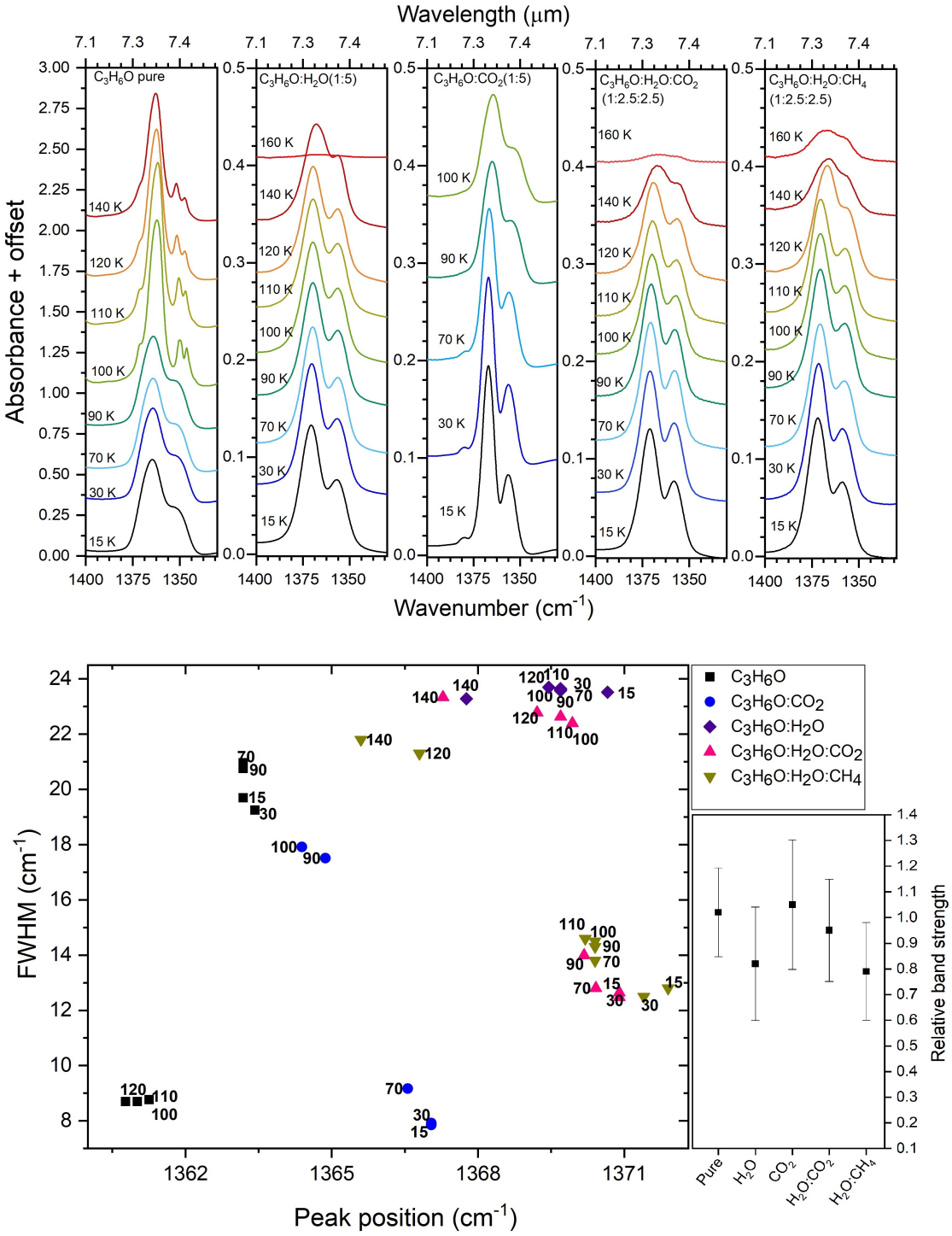

Fig. A.3. *Upper panel*: infrared spectra in the range of 1400–1300 cm^{-1} (7.10–7.69 μm) showing the CH_3 symmetric deformation band of acetone embedded in different ice mixtures, *from left to right*: pure CH_3COCH_3, CH_3COCH_3:H_2O(1:5), CH_3COCH_3:CO_2(1:5), CH_3COCH_3:H_2O:CO_2(1:2.5:2.5), and CH_3COCH_3:H_2O:CH_4(1:2.5:2.5). The spectra at different temperatures are offset for improved visualization. *Bottom left*: peak position vs. FWHM plot for the CH_3 symmetric deformation band in different ice matrices, represented by the different colors, and for different temperatures, indicated by the numbers in the graph. *Bottom right*: apparent band strength for the acetone CH_3 symmetric deformation band at 15 K in the various matrices with respect to the band strength for pure acetone from Hudson et al. (2018).

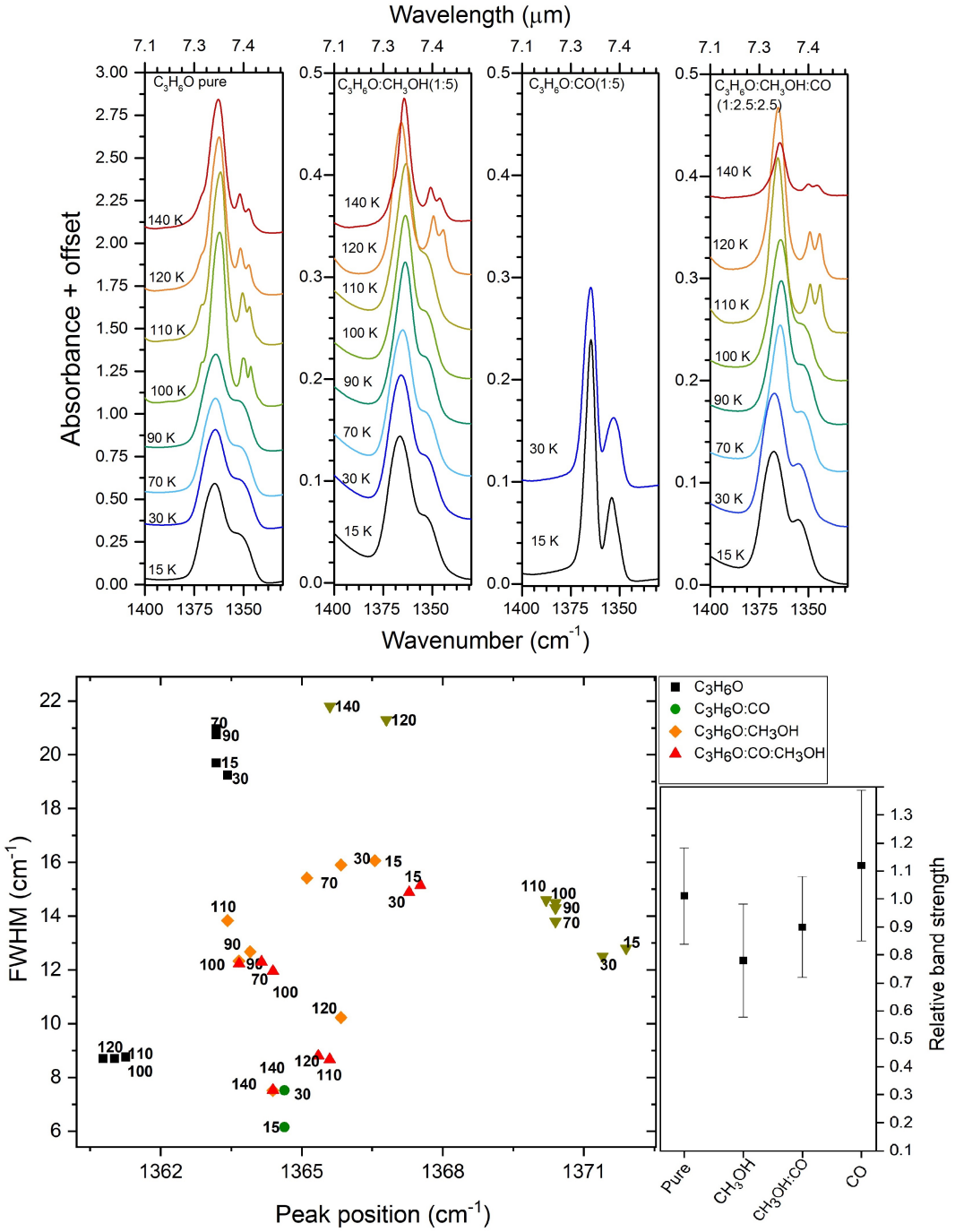

Fig. A.4. *Upper panel*: infrared spectra in the range of 1400–1300 cm^{-1} (7.10–7.69 μm) showing the CH_3 symmetric deformation band of acetone embedded in different ice mixtures, *from left to right*: pure CH_3COCH_3, CH_3COCH_3:CH_3OH(1:5), CH_3COCH_3:CO(1:5), and CH_3COCH_3:CH_3OH:CO(1:2.5:2.5). The spectra at different temperatures are offset for improved visualization. *Bottom left*: peak position vs. FWHM plot for the CH_3 symmetric deformation band in different ice matrices, represented by the different colors, and for different temperatures, indicated by the numbers in the graph. *Bottom right*: apparent band strength for the acetone CH_3 symmetric deformation band at 15 K in the various matrices with respect to the band strength for pure acetone from Hudson et al. (2018).

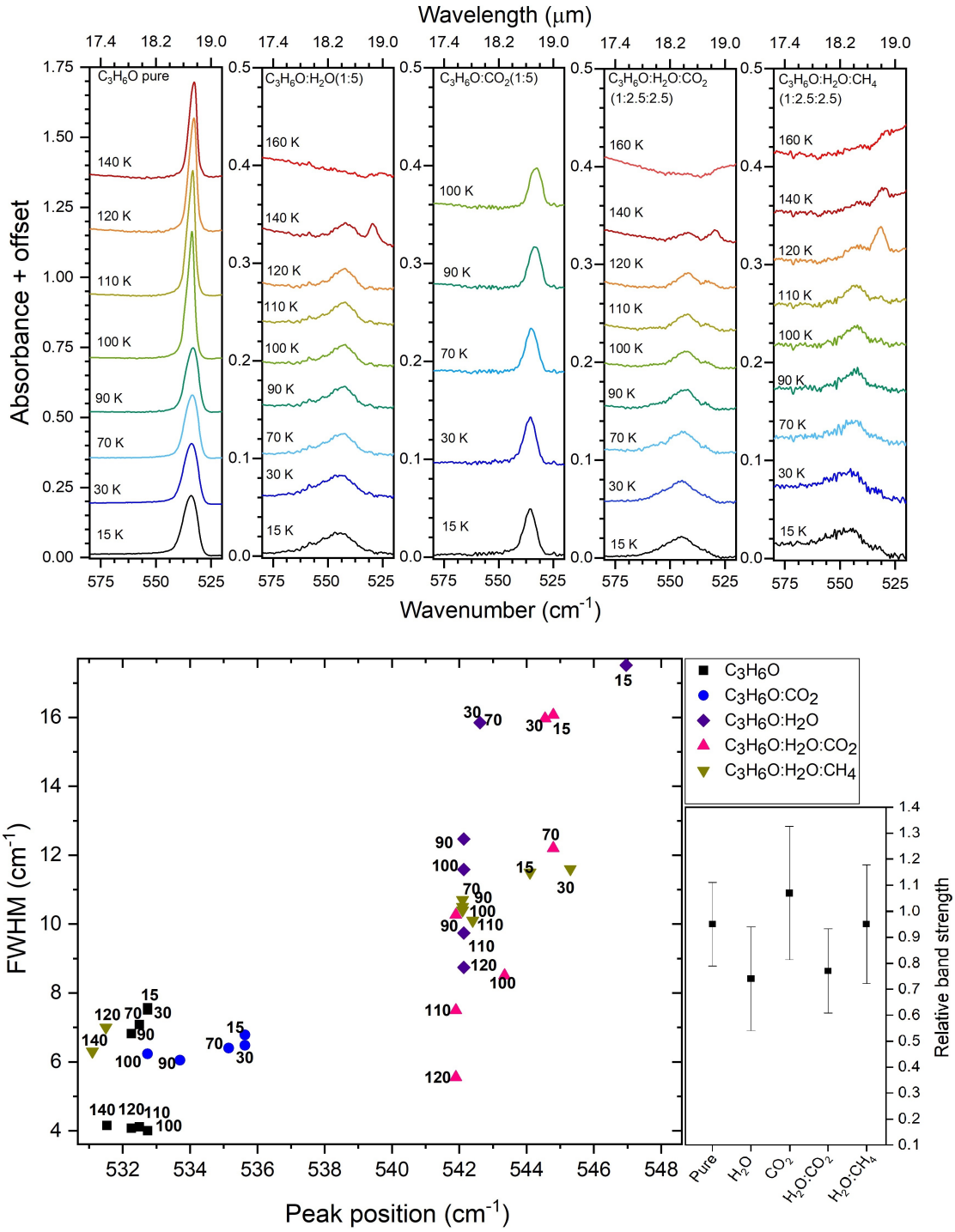

Fig. A.5. *Upper panel*: infrared spectra in the range of 520–580 cm^{-1} (19.2–17.2 μm) showing the CO in-plane deformation band of acetone in different ice mixtures, *from left to right*: pure CH_3COCH_3, CH_3COCH_3:H_2O(1:5), CH_3COCH_3:CO_2(1:5), CH_3COCH_3:H_2O:CO_2(1:2.5:2.5), and CH_3COCH_3:H_2O:CH_4(1:2.5:2.5). The spectra at different temperatures are offset for improved visualization. *Bottom left*: peak position vs. FWHM plot for the CO in-plane deformation band in different ice matrices, represented by the different colors, and for different temperatures, indicated by the numbers in the graph. *Bottom right*: apparent band strength for the acetone CO in-plane deformation band at 15 K in the various matrices with respect to the band strength for pure acetone from Hudson et al. (2018).

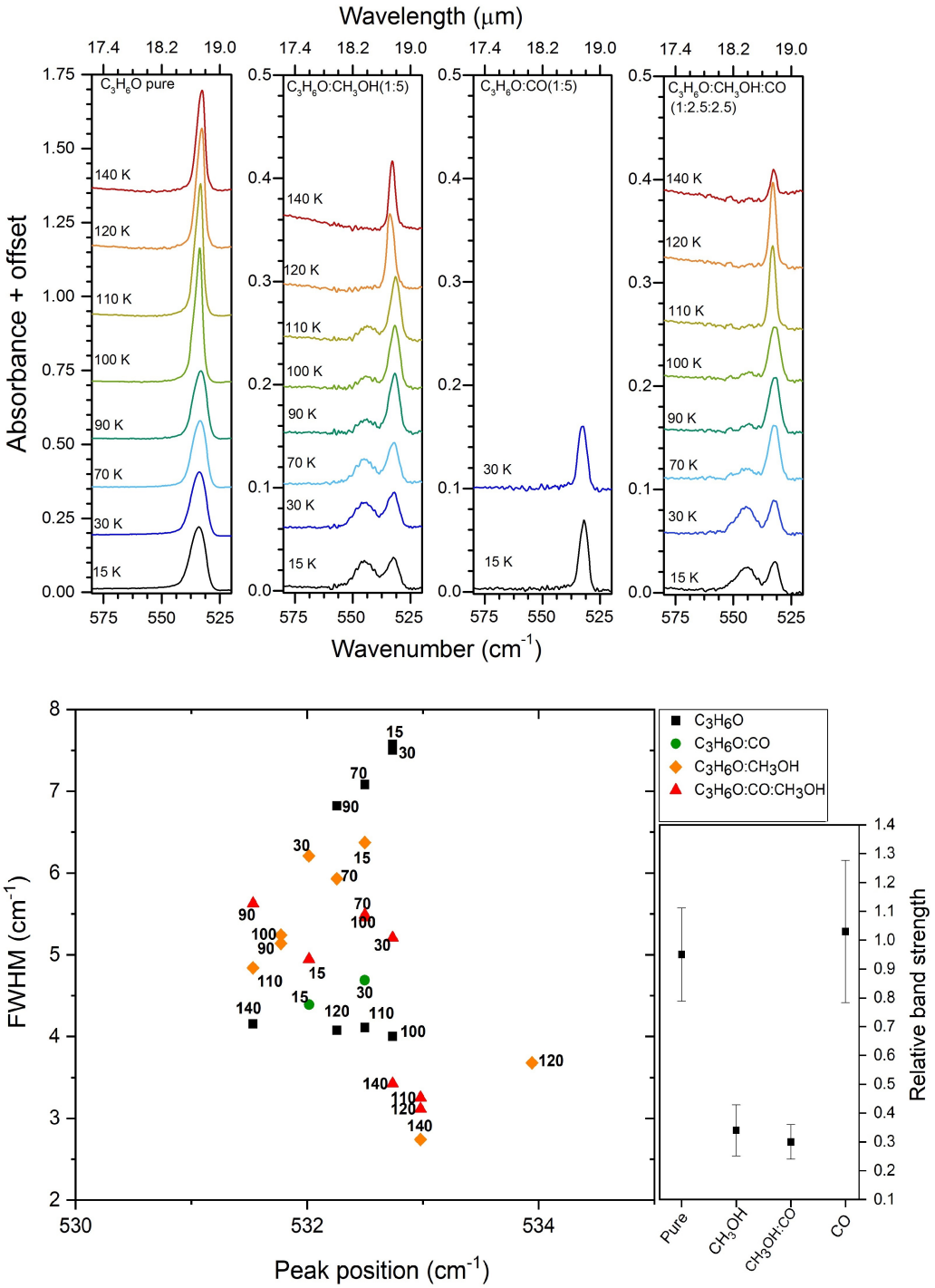

Fig. A.6. *Upper panel*: infrared spectra in the range of 520–580 cm^{-1} (19.2–17.2 μm) showing the CO in-plane deformation band of acetone in different ice mixtures, *from left to right*: pure CH_3COCH_3,CH_3COCH_3:CH_3OH(1:5), CH_3COCH_3:CO(1:5), and CH_3COCH_3:CH_3OH:CO(1:2.5:2.5). The spectra at different temperatures are offset for improved visualization. *Bottom left*: peak position vs. FWHM plot for the CO in-plane deformation band in different ice matrices, represented by the different colors, and for different temperatures, indicated by the numbers in the graph. *Bottom right*: apparent band strength for the acetone CO in-plane deformation band at 15 K in the various matrices with respect to the band strength for pure acetone from Hudson et al. (2018).

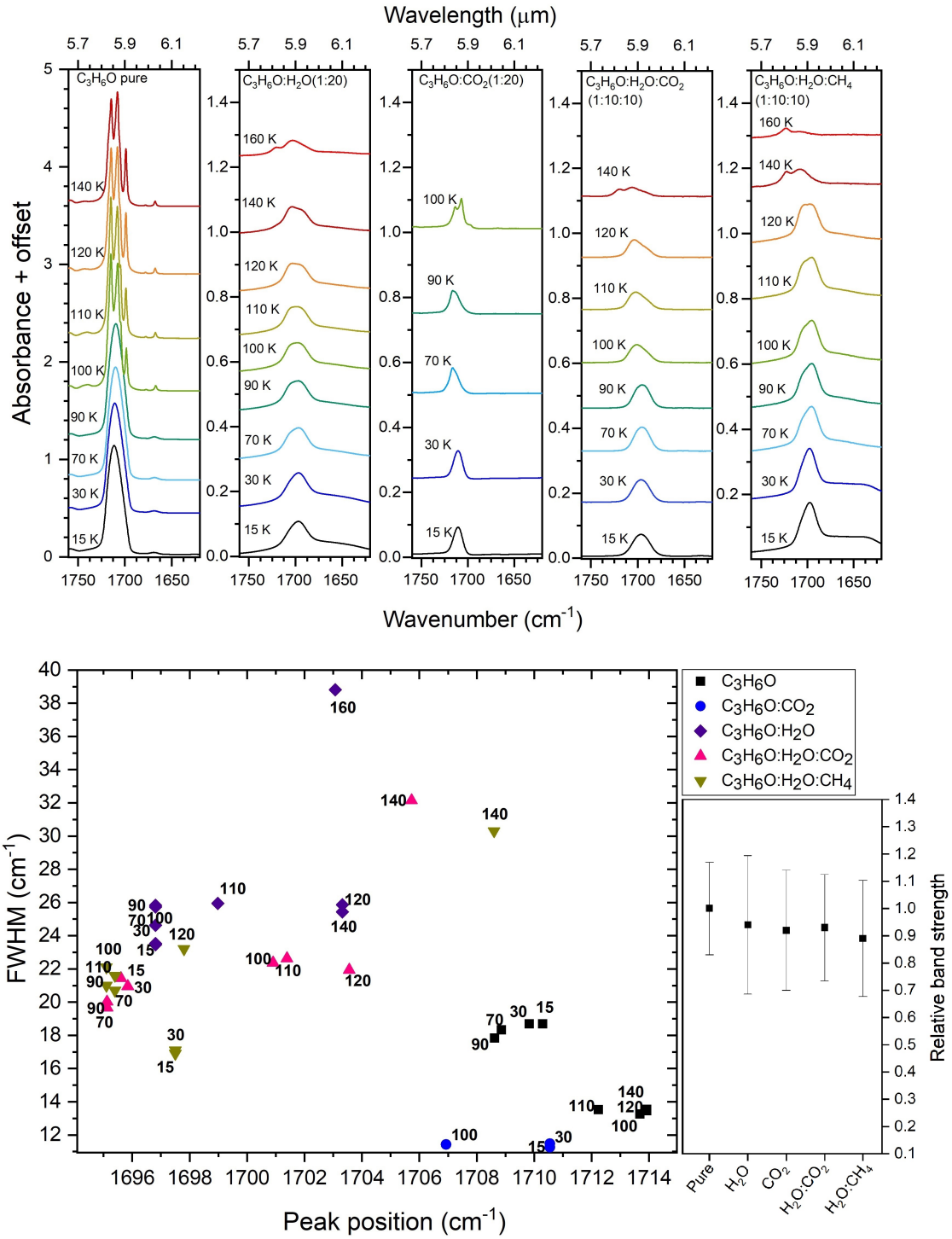

Fig. A.7. *Upper panel*: infrared spectra in the range of 1760–1630 cm^{-1} (5.68–6.13 μm) showing the C=O stretch band of acetone embedded in different ice mixtures, *from left to right*: pure CH_3COCH_3, CH_3COCH_3:H_2O(1:20), CH_3COCH_3:CO_2(1:20), CH_3COCH_3:H_2O:CO_2(1:10:10), and CH_3COCH_3:H_2O:CH_4(1:10:10). The spectra at different temperatures are offset for improved visualization. *Bottom left*: peak position vs. FWHM plot for the C=O stretch band in different ice matrices, represented by the different colors, and for different temperatures, indicated by the numbers in the graph. *Bottom right*: apparent band strength for the acetone C=O stretch band at 15 K in the various matrices with respect to the band strength for pure acetone from Hudson et al. (2018).

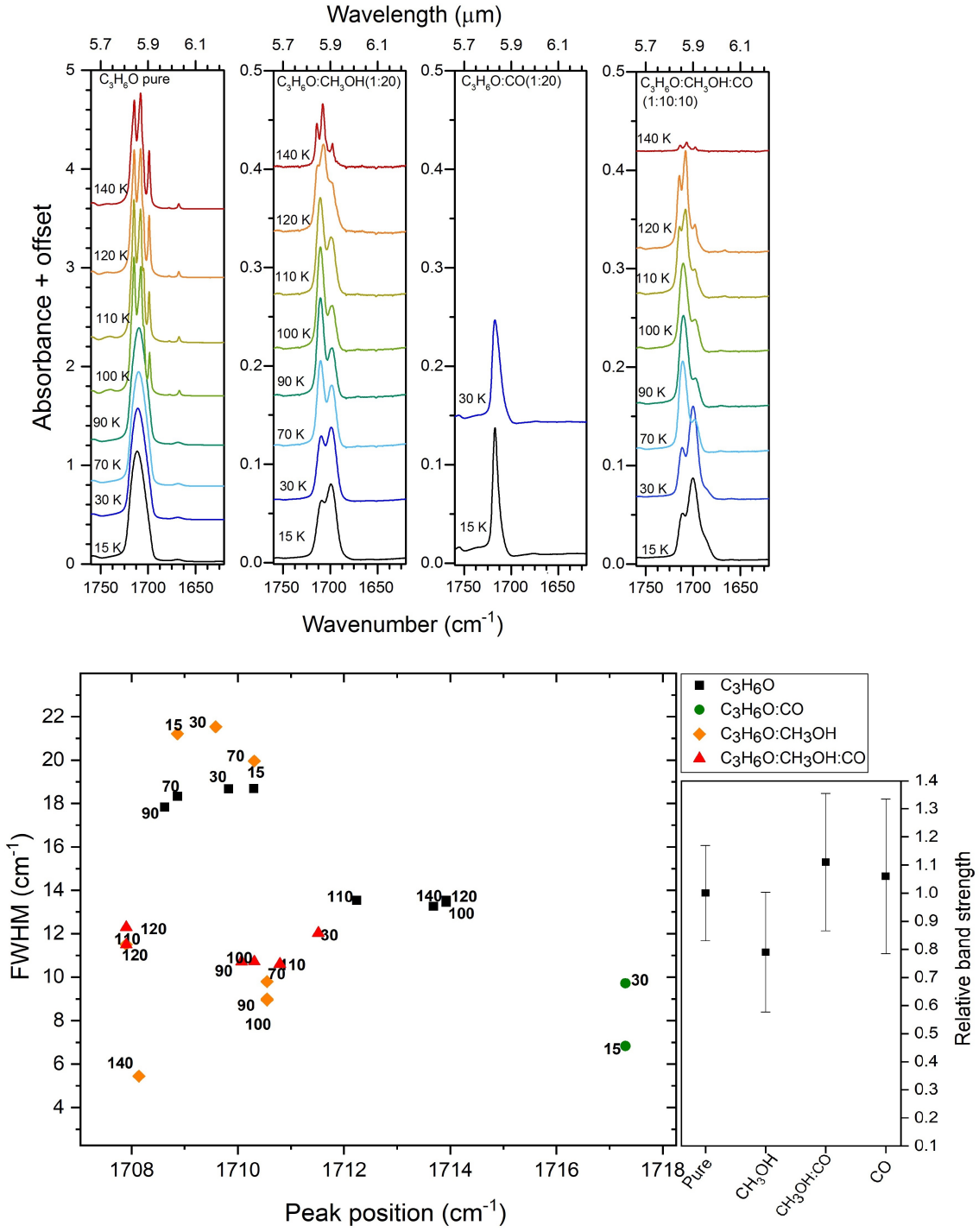

Fig. A.8. *Upper panel*: infrared spectra in the range of 1760–1630 cm^{-1} (5.68–6.13 μm) showing the C=O stretch band of acetone embedded in different ice mixtures, *from left to right*: pure CH_3COCH_3, CH_3COCH_3:CH_3OH(1:20), CH_3COCH_3:CO(1:20), and CH_3COCH_3:CH_3OH:CO(1:10:10). The spectra at different temperatures are offset for improved visualization. *Bottom left*: peak position vs. FWHM plot for the C=O stretch band in different ice matrices, represented by the different colors, and for different temperatures, indicated by the numbers in the graph. *Bottom right*: apparent band strength for the acetone C=O stretch band at 15 K in the various matrices with respect to the band strength for pure acetone from Hudson et al. (2018).

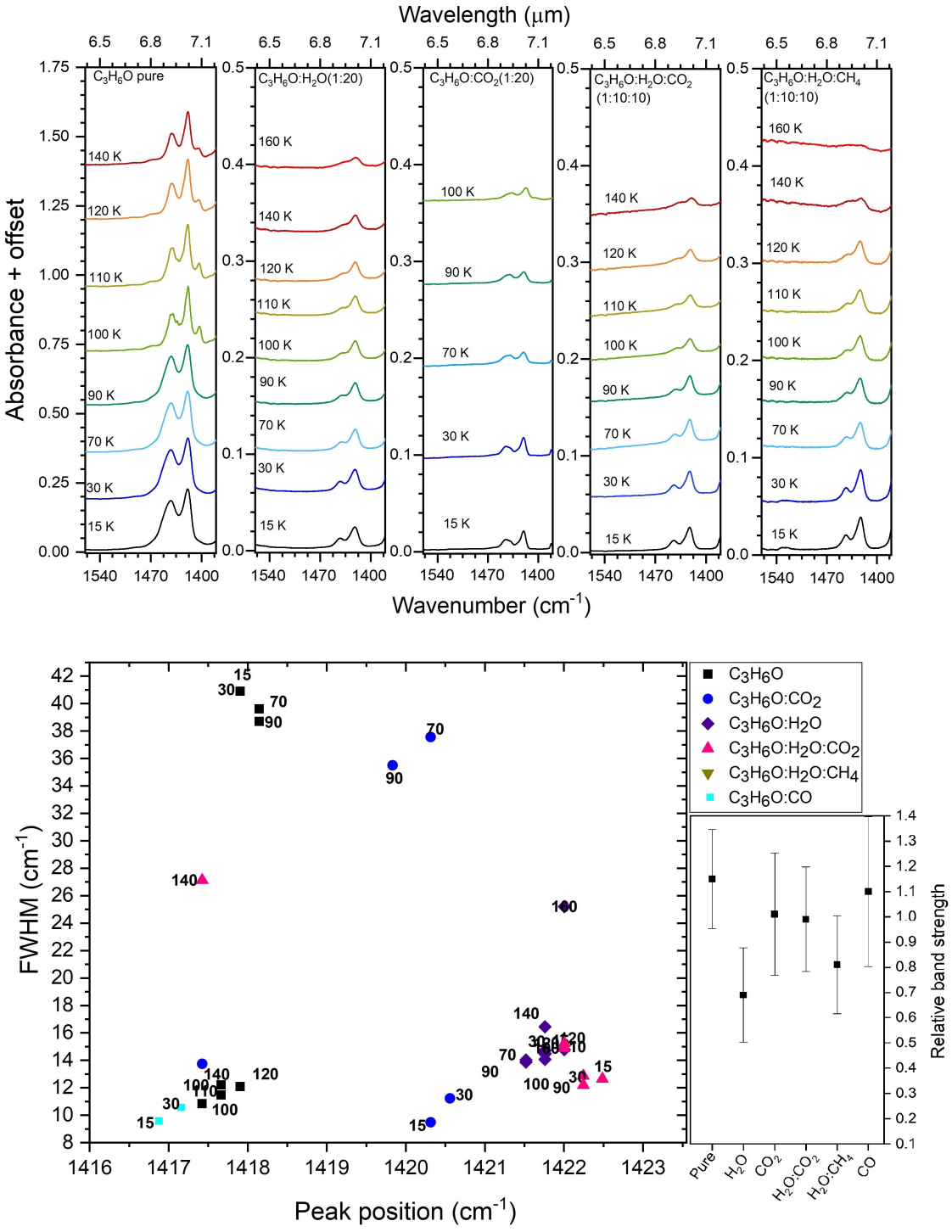

Fig. A.9. *Upper panel*: infrared spectra in the range of 1550–1390 cm^{-1} (6.45–7.19 μm) showing the CH_3 asymmetric deformation band of acetone embedded in different ice mixtures, *from left to right*: pure CH_3COCH_3, CH_3COCH_3:H_2O(1:20), CH_3COCH_3:CO_2(1:20), CH_3COCH_3:H_2O:CO_2(1:10:10), and CH_3COCH_3:H_2O:CH_4(1:10:10). The spectra at different temperatures are offset for improved visualization. *Bottom left*: peak position vs. FWHM plot for the CH_3 asymmetric deformation band in different ice matrices, represented by the different colors, and for different temperatures, indicated by the numbers in the graph. *Bottom right*: apparent band strength for the acetone CH_3 asymmetric deformation band at 15 K in the various matrices with respect to the band strength for pure acetone from Hudson et al. (2018).

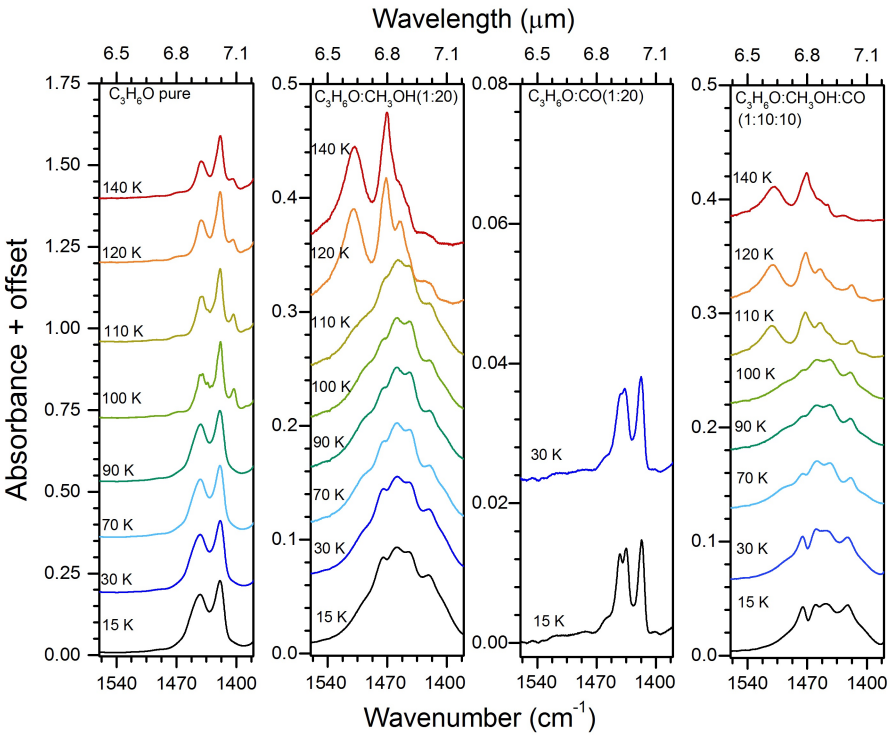

Fig. A.10. infrared spectra in the range of 1550–1390 cm^{-1} (6.45–7.19 μm) showing the CH_3 asymmetric deformation band of acetone embedded in different ice mixtures, *from left to right*: pure CH_3COCH_3, CH_3COCH_3:CH_3OH(1:20), CH_3COCH_3:CO(1:20), and CH_3COCH_3:CH_3OH:CO(1:10:10). The spectra at different temperatures are offset for improved visualization. Since the FWHM of the CH_3 asymmetric deformation band was not measured in the methanol-containing mixtures (due to the overlap with the methanol CH_3 bending mode), the peak position vs. FWHM plot for this acetone feature in CO matrix is displayed with the data in Fig. A.9.

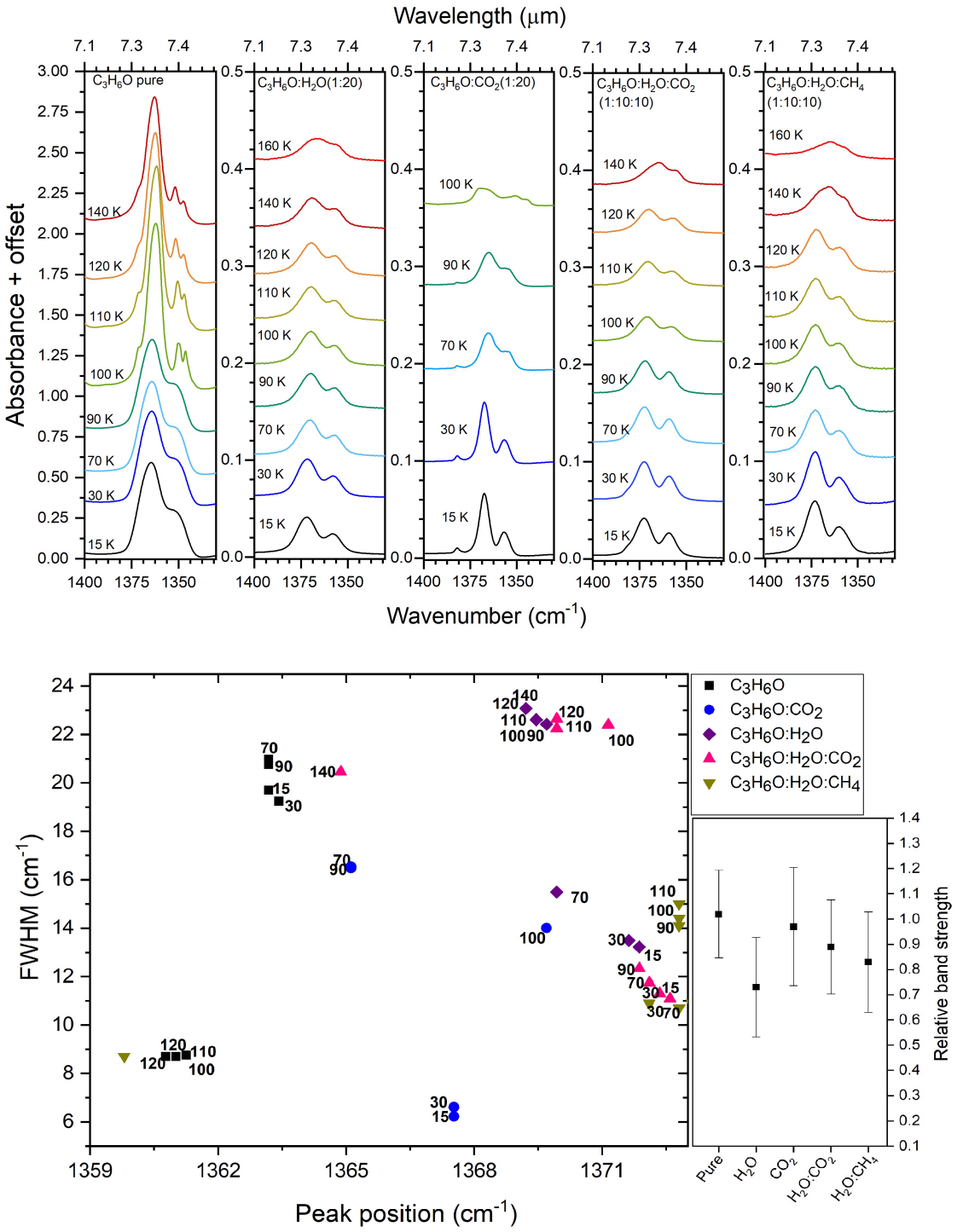

Fig. A.11. *Upper panel*: infrared spectra in the range of 1400–1300 cm^{-1} (7.10–7.69 μm) showing the CH_3 symmetric deformation band of acetone embedded in different ice mixtures, *from left to right*: pure CH_3COCH_3, CH_3COCH_3:H_2O(1:20), CH_3COCH_3:CO_2(1:20), CH_3COCH_3:H_2O:CO_2(1:10:10), and CH_3COCH_3:H_2O:CH_4(1:10:10). The spectra at different temperatures are offset for improved visualization. *Bottom left*: peak position vs. FWHM plot for the CH_3 symmetric deformation band in different ice matrices, represented by the different colors, and for different temperatures, indicated by the numbers in the graph. *Bottom right*: apparent band strength for the acetone CH_3 symmetric deformation band at 15 K in the various matrices with respect to the band strength for pure acetone from Hudson et al. (2018).

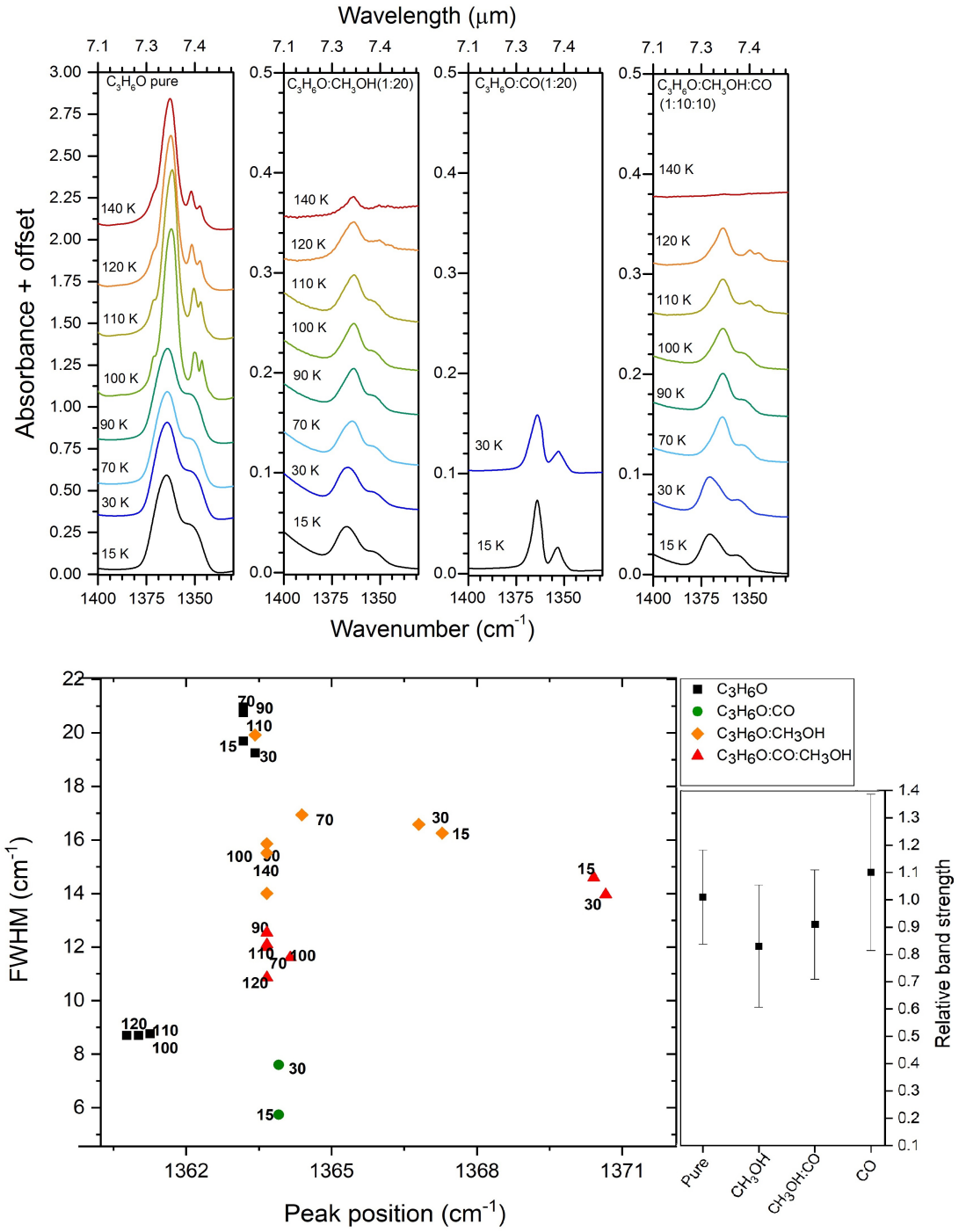

Fig. A.12. *Upper panel*: infrared spectra in the range of 1400–1300 cm^{-1} (7.10–7.69 μm) showing the CH_3 symmetric deformation band of acetone embedded in different ice mixtures, *from left to right*: pure CH_3COCH_3,CH_3COCH_3:CH_3OH(1:20), CH_3COCH_3:CO(1:20), and CH_3COCH_3:CH_3OH:CO(1:10:10). The spectra at different temperatures are offset for improved visualization. *Bottom left*: peak position vs. FWHM plot for the CH_3 symmetric deformation band in different ice matrices, represented by the different colors, and for different temperatures, indicated by the numbers in the graph. *Bottom right*: apparent band strength for the acetone CH_3 symmetric deformation band at 15 K in the various matrices with respect to the band strength for pure acetone from Hudson et al. (2018).

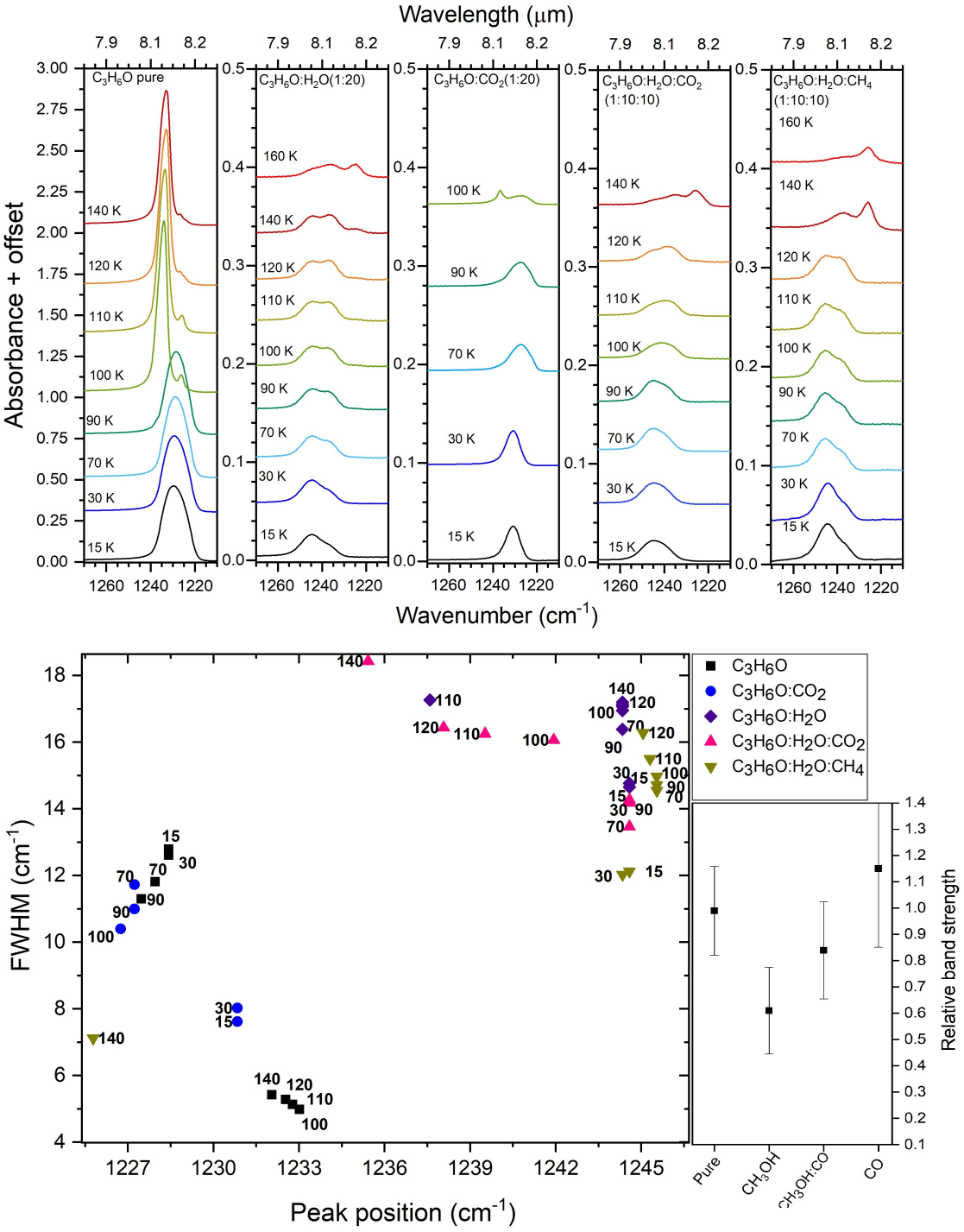

Fig. A.13. *Upper panel*: infrared spectra in the range of 1270–1210 cm^{-1} (7.87–8.26 μm) showing the CCC asymmetric stretch band of acetone in different ice mixtures, *from left to right*: pure CH_3COCH_3, CH_3COCH_3:H_2O(1:20), CH_3COCH_3:CO_2(1:20), CH_3COCH_3:H_2O:CO_2(1:10:10), and CH_3COCH_3:H_2O:CH_4(1:10:10). The spectra at different temperatures are offset for improved visualization. *Bottom left*: peak position vs. FWHM plot for the CCC asymmetric stretch band in different ice matrices, represented by the different colors, and for different temperatures, indicated by the numbers in the graph. *Bottom right*: apparent band strength for the acetone CCC asymmetric stretch band at 15 K in the various matrices with respect to the band strength for pure acetone from Hudson et al. (2018).

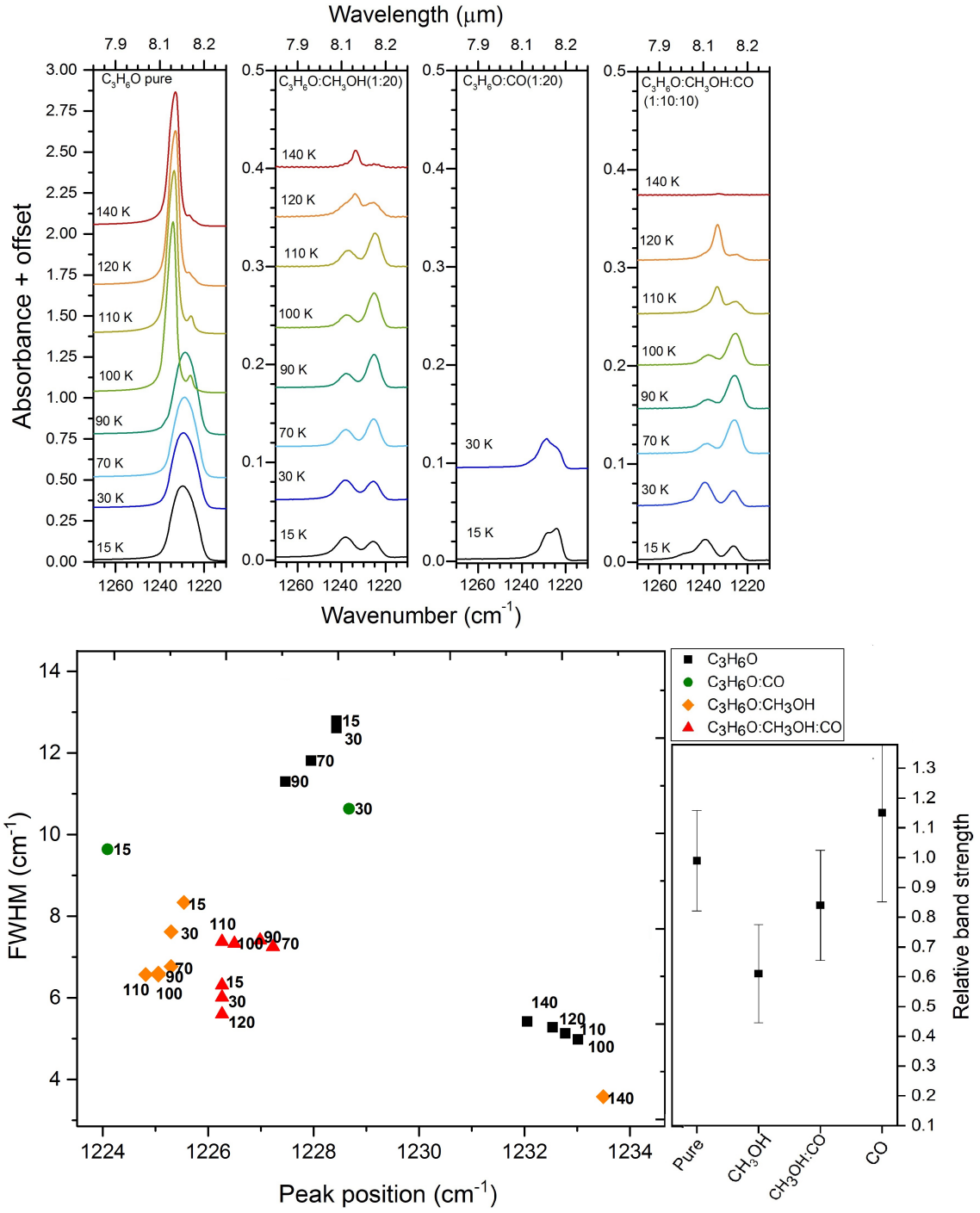

Fig. A.14. *Upper panel*: infrared spectra in the range of 1270–1210 cm^{-1} (7.87–8.26 μm) showing the CCC asymmetric stretch band of acetone in different ice mixtures, *from left to right*: pure CH_3COCH_3, CH_3COCH_3:CH_3OH(1:20), CH_3COCH_3:CO(1:20), and CH_3COCH_3:CH_3OH:CO(1:10:10). The spectra at different temperatures are offset for improved visualization. *Bottom left*: peak position vs. FWHM plot for the CCC asymmetric stretch band in different ice matrices, represented by the different colors, and for different temperatures, indicated by the numbers in the graph. *Bottom right*: apparent band strength for the acetone CCC asymmetric stretch band at 15 K in the various matrices with respect to the band strength for pure acetone from Hudson et al. (2018).

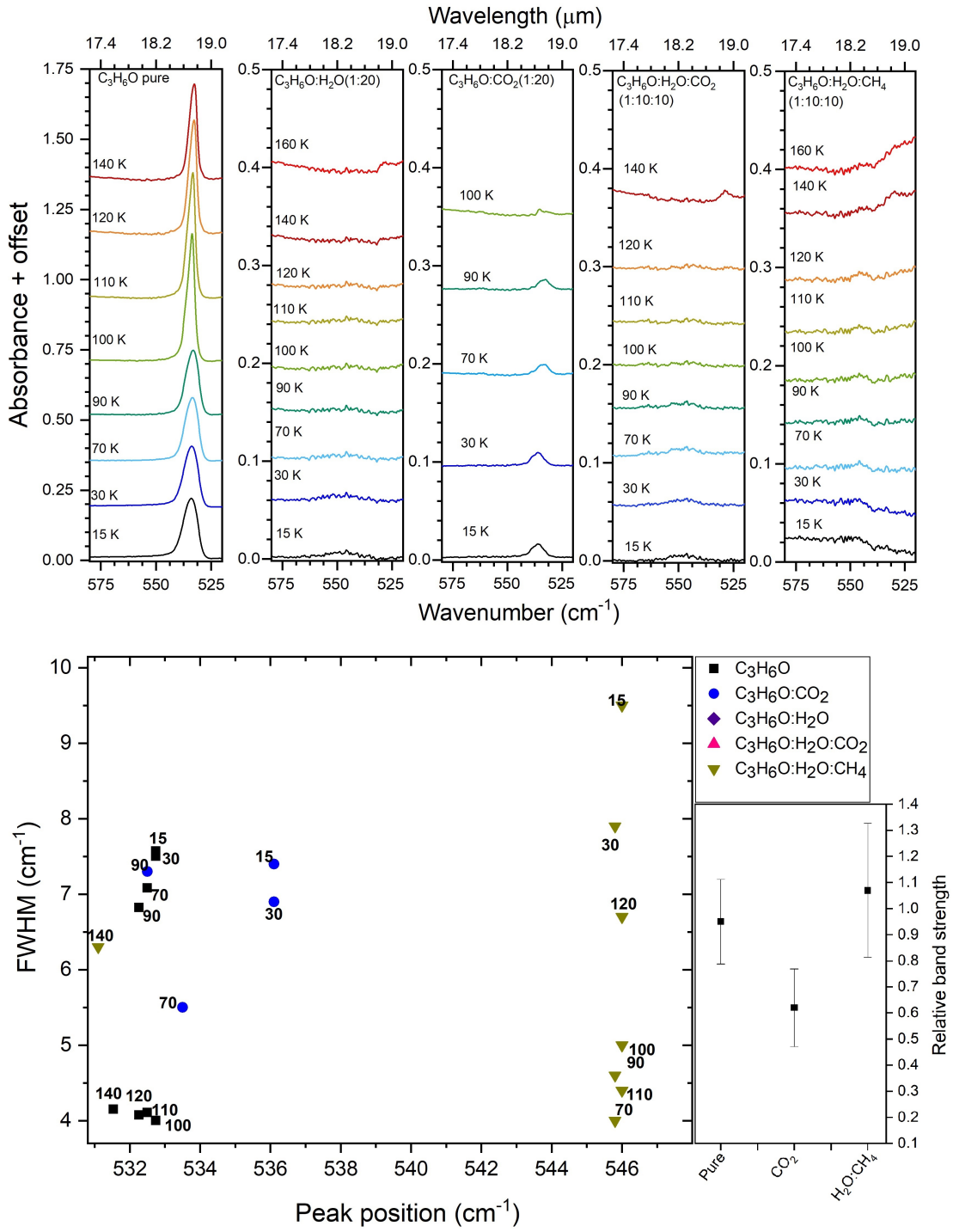

Fig. A.15. *Upper panel*: infrared spectra in the range of 520–580 cm^{-1} (19.2–17.2 μm) showing the CO in-plane deformation band of acetone in different ice mixtures, *from left to right*: pure CH_3COCH_3, CH_3COCH_3:H_2O(1:20), CH_3COCH_3:CO_2(1:20), CH_3COCH_3:H_2O:CO_2(1:10:10), and CH_3COCH_3:H_2O:CH_4(1:10:10). The spectra at different temperatures are offset for improved visualization. *Bottom left*: peak position vs. FWHM plot for the CO in-plane deformation band in different ice matrices, represented by the different colors, and for different temperatures, indicated by the numbers in the graph. *Bottom right*: apparent band strength for the acetone CO in-plane deformation band at 15 K in the various matrices with respect to the band strength for pure acetone from Hudson et al. (2018).

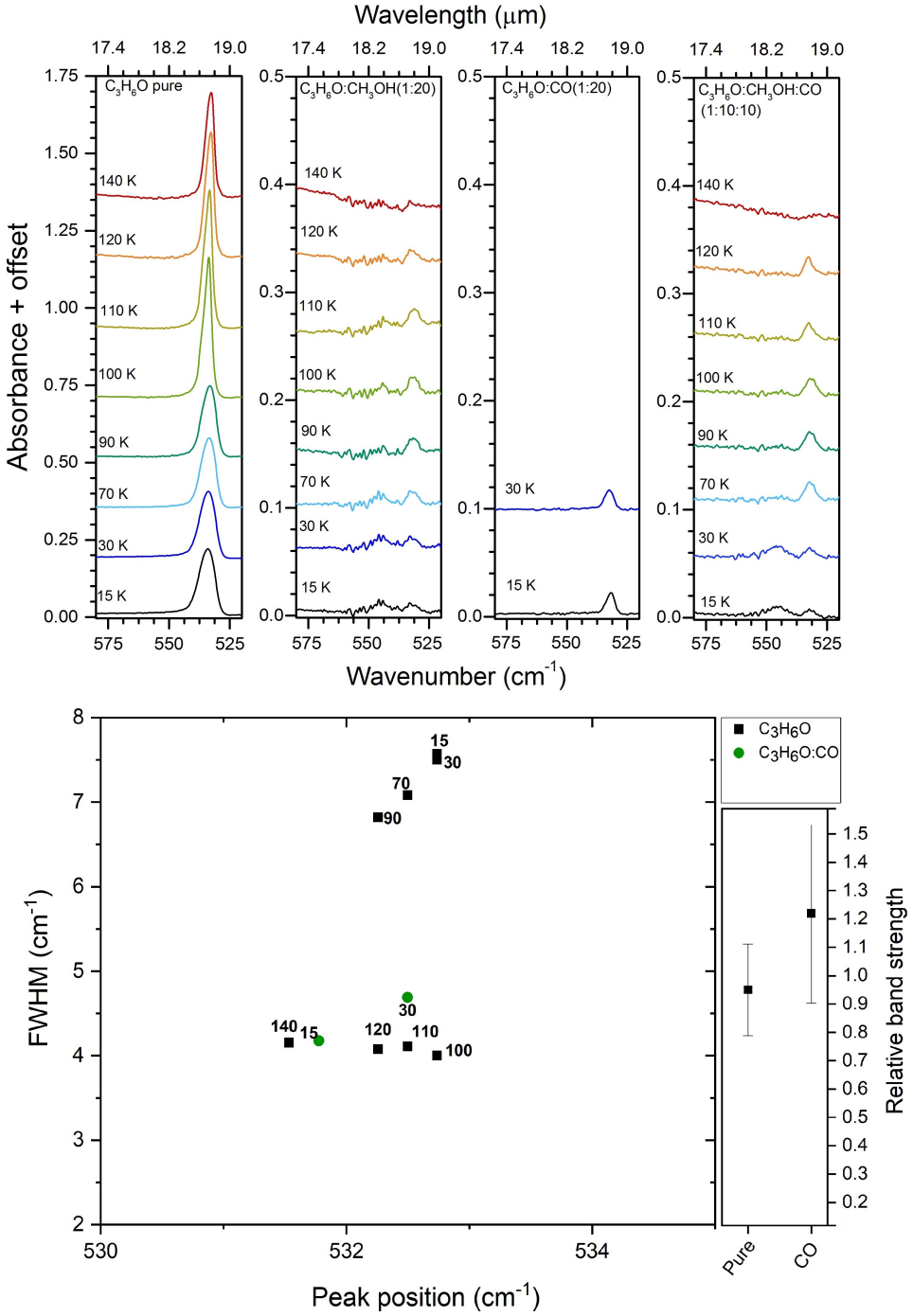

Fig. A.16. *Upper panel*: infrared spectra in the range of 520–580 cm^{-1} (19.2–17.2 μm) showing the CO in-plane deformation band of acetone in different ice mixtures, *from left to right*: pure CH_3COCH_3, CH_3COCH_3:CH_3OH(1:20), CH_3COCH_3:CO(1:20), and CH_3COCH_3:CH_3OH:CO(1:10:10). The spectra at different temperatures are offset for improved visualization. *Bottom left*: peak position vs. FWHM plot for the CO in-plane deformation band in different ice matrices, represented by the different colors, and for different temperatures, indicated by the numbers in the graph. *Bottom right*: apparent band strength for the acetone CO in-plane deformation band at 15 K in the various matrices with respect to the band strength for pure acetone from Hudson et al. (2018).

Appendix B: Ice band parameters

In this section, the peak position and the FWHM of the acetone bands discussed in the text and shown in Appendix A are presented in tables. The tables display the peak position for a given vibrational mode in the different ice matrices used in this work and at different temperatures, ranging from 15 K up to the matrix desorption temperature (Tables B.1–B.10).

An asterisk (*) denotes that the FWHM is the value derived for a blending of two or more peaks. The general uncertainty of the peak position is about 0.5 cm^{-1} for all the measurements and the typical error of the FWHM values amounts to 0.8 cm^{-1}.

Table B.1. Peak position and FWHM of the acetone CO-stretch mode for pure acetone and mixtures with acetone ratio 1:5 and for temperatures ranging from 15 K to 140 K. See also Figs. 2 and 3.

Mixture	Temperature	Peak position		*FWHM*	
	(K)	(cm^{-1})	(μm)	(cm^{-1})	(μm)
CH_3COCH_3		1710.3	5.847	18.7	0.0640
CH_3COCH_3:CO		1715.9	5.828	8.5	0.0289
CH_3COCH_3:CO_2		1710.8	5.845	12.9	0.0440
CH_3COCH_3:H_2O		1700.2	5.882	27.8	0.0965*
CH_3COCH_3:CH_3OH	15	1699.5	5.884	–	–
		1708.9	5.851	23.8	0.0819
CH_3COCH_3:H_2O:CO_2		1699.9	5.882	22.4	0.0776
CH_3COCH_3:H_2O:CH_4		1701.6	5.877	22.0	–
CH_3COCH_3:CH_3OH:CO		1700.4	5.881	–	–
		1710.3	5.847	23.7	0.0815*
CH_3COCH_3		1709.8	5.848	18.7	0.064
CH_3COCH_3:CO		1715.4	5.829	10.7	0.0364
CH_3COCH_3:CO_2		1710.8	5.845	12.7	0.0433
CH_3COCH_3:H_2O		1701.1	5.878	27.7	0.0959
CH_3COCH_3:CH_3OH	30	1698.7	5.887	–	–
		1709.0	5.851	23.3	0.080*
CH_3COCH_3:H_2O:CO_2		1699.7	5.883	21.9	0.0759
CH_3COCH_3:H_2O:CH_4		1701.4	5.877	21.5	–
CH_3COCH_3:CH_3OH:CO		1699.9	5.882	–	–
		1710.6	5.846	23.1	0.0794*
CH_3COCH_3		1708.9	5.852	18.3	0.0628
CH_3COCH_3:CO		–	–	–	–
CH_3COCH_3:CO_2		1710.8	5.845	12.8	0.0439
CH_3COCH_3:H_2O		1701.1	5.878	26.7	0.092
CH_3COCH_3:CH_3OH	70	1698.5	5.887	–	–
		1709.6	5.849	22.5	0.0776*
CH_3COCH_3:H_2O:CO_2		1699.5	5.884	20.5	0.0709*
CH_3COCH_3:H_2O:CH_4		1702.3	5.874	21.4	–
CH_3COCH_3:CH_3OH:CO		1710.3	5.847	14.2	0.0486
CH_3COCH_3		1708.6	5.853	17.8	0.0611
CH_3COCH_3:CO		–	–	–	–
CH_3COCH_3:CO_2		1712.0	5.841	14.7	0.0503
CH_3COCH_3:H_2O		1701.6	5.877	26.0	0.0901
CH_3COCH_3:CH_3OH	90	1710.1	5.848	12.3	0.0422*
CH_3COCH_3:H_2O:CO_2		1700.4	5.881	20.0	0.0692
CH_3COCH_3:H_2O:CH_4		1702.8	5.873	20.4	–
CH_3COCH_3:CH_3OH:CO		1709.6	5.849	14.4	0.0493
CH_3COCH_3		1697.5	5.891	–	–
		1706.7	5.859	–	–
		1713.9	5.835	13.5	0.0463*
CH_3COCH_3:CO		–	–	–	–
CH_3COCH_3:CO_2		1712.2	5.840	15.5	0.0532
CH_3COCH_3:H_2O	100	1701.9	5.876	25.6	0.0888
CH_3COCH_3:CH_3OH		1710.1	5.848	12.3	0.0422
CH_3COCH_3:H_2O:CO_2		1701.4	5.877	20.0	0.0691
CH_3COCH_3:H_2O:CH_4		1703.3	5.871	19.8	–
CH_3COCH_3:CH_3OH:CO		1709.3	5.850	14.1	0.0482
CH_3COCH_3		1697.8	5.890	–	–
		1706.9	5.858	–	–
		1713.9	5.835	13.5	0.0463*
CH_3COCH_3:CO		–	–	–	–
CH_3COCH_3:CO_2		–	–	–	–
CH_3COCH_3:H_2O	110	1702.1	5.875	25.0	0.0868
CH_3COCH_3:CH_3OH		1710.1	5.847	13.0	0.0442
CH_3COCH_3:H_2O:CO_2		1701.6	5.877	20.0	0.0689

Table B.1. continued.

Mixture	Temperature	Peak position		*FWHM*	
	(K)	(cm^{-1})	(μm)	(cm^{-1})	(μm)
CH_3COCH_3:H_2O:CH_4		1703.3	5.871	19.4	–
CH_3COCH_3:CH_3OH:CO		1706.9	5.858	11.3	0.0387
		1714.2	5.834	–	–
CH_3COCH_3		1698.0	5.889	–	–
		1706.9	5.858	–	–
		1713.9	5.835	13.5	0.0460*
CH_3COCH_3:CO		–	–	–	–
CH_3COCH_3:CO_2		–	–	–	–
CH_3COCH_3:H_2O	120	1702.1	5.875	24.3	0.0843*
CH_3COCH_3:CH_3OH		1706.0	5.862	12.8	0.0439*
		1713.7	5.835	5.7	0.0196
CH_3COCH_3:H_2O:CO_2		1702.1	5.875	20.2	0.0698
CH_3COCH_3:H_2O:CH_4		1709.8	5.849	22.8	–
CH_3COCH_3:CH_3OH:CO		1706.9	5.859	–	–
		1714.2	5.834	11.2	0.0384
CH_3COCH_3		1698.0	5.889	–	–
		1706.9	5.858	–	–
		1713.7	5.835	13.3	0.0453*
CH_3COCH_3:CO		–	–	–	–
CH_3COCH_3:CO_2		–	–	–	–
CH_3COCH_3:H_2O		1703.8	5.869	21.7	0.0749*
CH_3COCH_3:CH_3OH	140	1698.0	5.889	–	–
		1707.4	5.857	5.9	0.0202*
		1714.2	5.834	11.8	0.0402*
CH_3COCH_3:H_2O:CO_2		1703.6	5.870	21.1	0.0724
CH_3COCH_3:H_2O:CH_4		1707.4	5.857	23.5	–
CH_3COCH_3:CH_3OH:CO		1707.9	5.855	–	–
		1714.2	5.834	5.7	0.0196

Table B.2. Peak position and FWHM of the acetone CH_3 asymmetric deformation mode for pure acetone and mixtures with acetone ratio 1:5 and for temperatures ranging from 15 K to 140 K. See also Figs. A.1 and A.2.

Mixture	Temperature	Peak position		*FWHM*	
	(K)	(cm^{-1})	(μm)	(cm^{-1})	(μm)
CH_3COCH_3		1417.9	7.0527	40.9	0.199*
		1441.0	6.9394	–	–
CH_3COCH_3:CO		1417.4	7.0551	8.7	0.0434
		1436.7	6.9604	15.1	0.0776*
CH_3COCH_3:CO_2	15	1419.8	7.0431	11.4	0.0563
		1444.2	6.9243	–	–
CH_3COCH_3:H_2O		1421.5	7.0347	20.0	0.100*
		1442.7	6.9313	–	–
CH_3COCH_3:H_2O:CO_2		1422.0	7.0323	16.3	0.0804
		1444.4	6.9232	–	–
CH_3COCH_3:H_2O:CH_4		1422.5	7.0299	15.7	
		1443.0	6.930	14.2	
CH_3COCH_3		1417.9	7.0527	40.9	0.199*
		1441.3	6.9382	–	–
CH_3COCH_3:CO		1417.9	7.0527	8.7	0.0433
		1437.7	6.9557	14.2	0.0740
CH_3COCH_3:CO_2	30	1419.8	7.0431	11.3	0.0559
		1443.9	6.9255	–	–
CH_3COCH_3:H_2O		1421.0	7.0371	18.7	0.0923
		1441.3	6.9382	–	–
CH_3COCH_3:H_2O:CO_2		1421.8	7.0335	16.1	0.0792*
		1444.2	6.9243	–	–
CH_3COCH_3:H_2O:CH_4		1422.2	7.0314	15.3	
		1442.7	6.9315	14.3	
CH_3COCH_3		1418.1	7.0515	39.6	0.193*
		1441.0	6.9394	–	–
CH_3COCH_3:CO		–	–	–	–

Table B.2. continued.

Mixture	Temperature	Peak position		*FWHM*	
	(K)	(cm^{-1})	(μm)	(cm^{-1})	(μm)
CH_3COCH_3:CO_2		1419.8	7.0431	12.5	0.0621
		1441.8	6.9359	–	–
CH_3COCH_3:H_2O	70	1421.0	7.0371	18.7	0.0923
		1441.3	6.9382	–	–
CH_3COCH_3:H_2O:CO_2		1421.8	7.0335	15.6	0.0770*
		1442.3	6.9336	–	–
CH_3COCH_3:H_2O:CH_4		1422.2	7.0314	16.5	
		1442.5	6.9324	14.3	
CH_3COCH_3		1418.1	7.0515	38.7	0.189*
		1440.8	6.9406	–	–
CH_3COCH_3:CO		–	–	–	–
CH_3COCH_3:CO_2		1419.4	7.0455	15.6	0.0774
		1440.6	6.9417	–	–
CH_3COCH_3:H_2O	90	1421.0	7.0371	18.5	0.0911
		1439.5	6.9469	–	–
CH_3COCH_3:H_2O:CO_2		1421.5	7.0347	15.8	0.0781*
		1442.0	6.9348	–	–
CH_3COCH_3:H_2O:CH_4		1421.8	7.0333	16.3	
		1441.3	6.9381	14.4	
CH_3COCH_3		1401.8	7.1339	–	–
		1417.4	7.0551	10.8	0.0538
		1438.4	6.9522	–	–
CH_3COCH_3:CO		–	–	–	–
CH_3COCH_3:CO_2	100	1418.9	7.0479	36.3	0.177*
		1440.1	6.9440	–	–
CH_3COCH_3:H_2O		1421.0	7.0371	18.4	0.0906
		1439.1	6.9486	–	–
CH_3COCH_3:H_2O:CO_2		1420.8	7.0383	–	–
		1440.1	6.9440	17.2	0.0849*
CH_3COCH_3:H_2O:CH_4		1421.8	7.0333	16.4	
		1441.3	6.9382	14.2	
CH_3COCH_3		1402.2	7.1315	–	–
		1417.7	7.0539	11.5	0.0569
		1439.0	6.9495	–	–
CH_3COCH_3:CO		–	–	–	–
CH_3COCH_3:CO_2		–	–	–	–
CH_3COCH_3:H_2O	110	1421.3	7.0359	18.5	0.0910
		1440.0	6.9445	–	–
CH_3COCH_3:H_2O:CO_2		1420.8	7.0383	–	–
		1440.1	6.9440	18.8	0.0925*
CH_3COCH_3:H_2O:CH_4		1421.8	7.0333	16.4	
		1441.3	6.9382	14.4	
CH_3COCH_3		1402.5	7.1302	–	–
		1417.9	7.0527	12.1	0.0599
		1438.6	6.9510	–	–
CH_3COCH_3:CO		–	–	–	–
CH_3COCH_3:CO_2	120	–	–	–	–
CH_3COCH_3:H_2O		1421.0	7.0371	18.5	0.0913
		1439.5	6.9466	–	–
CH_3COCH_3:H_2O:CO_2		1420.6	7.0395	–	–
		1439.8	6.9452	19.7	0.0971*
CH_3COCH_3:H_2O:CH_4		1421.3	7.0358	30.0	
		1439.6	6.9463	18.0	
CH_3COCH_3		1404.9	7.1180	–	–
		1417.7	7.0539	12.2	0.0607
		1439.8	6.9452	–	–
CH_3COCH_3:CO		–	–	–	–
CH_3COCH_3:CO_2	140	–	–	–	–
CH_3COCH_3:H_2O		1420.3	7.0407	25.8	0.127
CH_3COCH_3:H_2O:CO_2		1420.3	7.0407	–	–
		1431.2	6.9873	29.4	0.144*
CH_3COCH_3:H_2O:CH_4		1421.5	7.0348	29.7	

Table B.3. Peak position and FWHM of the acetone CH_3 symmetric deformation mode for pure acetone and mixtures with acetone ratio 1:5 and for temperatures ranging from 15 K to 140 K. See also Figs. A.3 and A.4

Mixture	Temperature	Peak position		*FWHM*	
	(K)	(cm^{-1})	(μm)	(cm^{-1})	(μm)
CH_3COCH_3		1363.4	7.3345	19.2	0.0640
CH_3COCH_3:CO		1354.0	7.3854	7.7	0.0420
		1364.6	7.3280	6.2	0.0330
CH_3COCH_3:CO_2		1356.4	7.3723	–	–
		1367.0	7.3151	7.8	0.0420
CH_3COCH_3:H_2O	15	1356.9	7.3696	–	–
		1370.7	7.2958	23.5	0.127*
CH_3COCH_3:CH_3OH		1366.6	7.3176	16.1	0.0861
CH_3COCH_3:H_2O:CO_2		1358.1	7.3631	–	–
		1370.9	7.2945	12.6	0.0640
CH_3COCH_3:H_2O:CH_4		1358.8	7.3594	10.6	
		1371.9	7.2892	12.8	
CH_3COCH_3:CH_3OH:CO		1355.2	7.3788	–	–
		1367.5	7.3125	15.1	0.0810
CH_3COCH_3		1363.2	7.3358	19.7	0.106
CH_3COCH_3:CO		1353.1	7.3907	–	–
		1364.6	7.3280	7.5	0.0404
CH_3COCH_3:CO_2		1356.2	7.3736	–	–
		1367.0	7.3151	7.9	0.0424
CH_3COCH_3:H_2O	30	1356.4	7.3723	–	–
		1369.7	7.3009	23.6	0.127*
CH_3COCH_3:CH_3OH		1365.8	7.3215	15.9	0.0853
CH_3COCH_3:H_2O:CO_2		1358.1	7.3631	–	–
		1370.9	7.2945	12.5	0.0664
CH_3COCH_3:H_2O:CH_4		1358.8	7.3594	10.6	
		1371.4	7.2918	12.5	
CH_3COCH_3:CH_3OH:CO		1355.0	7.3801	–	–
		1367.3	7.3138	14.9	0.0796
CH_3COCH_3		1363.2	7.3358	20.8	0.112
CH_3COCH_3:CO		–	–	–	–
CH_3COCH_3:CO_2		1356.0	7.3749	–	–
		1366.6	7.3176	9.2	0.0491
CH_3COCH_3:H_2O	70	1356.4	7.3723	–	–
		1369.7	7.3009	23.6	0.127*
CH_3COCH_3:CH_3OH		1365.1	7.3254	15.4	0.0827
CH_3COCH_3:H_2O:CO_2		1357.9	7.3644	–	–
		1370.4	7.2970	12.8	0.0682
CH_3COCH_3:H_2O:CH_4		1357.4	7.367	10.4	
		1370.4	7.2971	13.8	
CH_3COCH_3:CH_3OH:CO		1353.8	7.3867	–	–
		1364.4	7.3293	12.0	0.0642
CH_3COCH_3		1363.2	7.3358	21.0	0.113
CH_3COCH_3:CO		–	–	–	–
CH_3COCH_3:CO_2		1364.9	7.3267	17.5	0.0944*
CH_3COCH_3:H_2O		1356.4	7.3723	–	–
		1369.7	7.3009	23.6	0.127*
CH_3COCH_3:CH_3OH	90	1363.9	7.3319	12.7	0.0681
CH_3COCH_3:H_2O:CO_2		1357.6	7.3657	–	–
		1370.2	7.2983	14.0	0.0746
CH_3COCH_3:H_2O:CH_4		1357.4	7.367	10.4	
		1370.4	7.2971	14.3	
CH_3COCH_3:CH_3OH:CO		1353.7	7.3869	–	–
		1363.7	7.3332	12.2	0.0657
CH_3COCH_3		1345.3	7.4330	7.7	0.0424*
		1349.2	7.4118	–	–
		1361.3	7.3462	8.8	0.0472
CH_3COCH_3:CO		–	–	–	–
CH_3COCH_3:CO_2		1364.4	7.3293	17.9	0.0966*
CH_3COCH_3:H_2O		1356.4	7.3723	–	–
		1369.7	7.3009	23.6	0.127*
CH_3COCH_3:CH_3OH	100	1363.7	7.3332	12.3	0.0662
CH_3COCH_3:H_2O:CO_2		1356.9	7.3696	–	–
		1369.9	7.2996	22.4	0.120*
CH_3COCH_3:H_2O:CH_4		1357.4	7.367	10.3	
		1370.4	7.2971	14.5	
CH_3COCH_3:CH_3OH:CO		1364.1	7.3306	12.3	0.0661

Table B.3. continued.

Mixture	Temperature	Peak position		*FWHM*	
	(K)	(cm^{-1})	(μm)	(cm^{-1})	(μm)
CH_3COCH_3		1345.6	7.4317	7.5	0.0413*
		1349.2	7.4118	–	–
		1361.0	7.3475	8.7	0.0471
CH_3COCH_3:CO		–	–	–	–
CH_3COCH_3:CO_2		–	–	–	–
CH_3COCH_3:H_2O	110	1356.4	7.3723	–	–
		1369.7	7.3009	23.6	0.127*
CH_3COCH_3:CH_3OH		1363.4	7.3345	13.8	0.0745
CH_3COCH_3:H_2O:CO_2		1356.7	7.3710	–	–
		1369.7	7.3009	22.6	0.1215*
CH_3COCH_3:H_2O:CH_4		1357.4	7.367	10.2	
		1370.2	7.2982	14.6	
CH_3COCH_3:CH_3OH:CO		1344.1	7.4397	–	–
		1349.0	7.4131	–	–
		1365.6	7.3228	8.7	0.047
CH_3COCH_3		1346.1	7.4290	7.3	0.0404*
		1349.4	7.4105	–	–
		1360.8	7.3488	8.7	0.0470
CH_3COCH_3:CO		–	–	–	–
CH_3COCH_3:CO_2		–	–	–	–
CH_3COCH_3:H_2O		1356.4	7.3723		–
		1369.5	7.3022	23.7	0.127*
CH_3COCH_3:CH_3OH	120	1344.4	7.4384	–	–
		1349.2	7.4118	–	–
		1365.8	7.3215	10.2	0.0548
CH_3COCH_3:H_2O:CO_2		1356.7	7.3710	–	–
		1369.2	7.3035	22.8	0.122*
CH_3COCH_3:H_2O:CH_4		1366.8	7.3163	21.3	
CH_3COCH_3:CH_3OH:CO		1344.1	7.4397	–	–
		1349.2	7.4118	–	–
		1365.4	7.3241	8.8	0.0472
CH_3COCH_3		1346.6	7.4264	–	–
		1350.9	7.4025	–	–
		1361.7	7.3436	9.3	0.0499
CH_3COCH_3:CO		–	–	–	–
CH_3COCH_3:CO_2		–	–	–	–
CH_3COCH_3:H_2O		1356.4	7.3723	–	–
		1367.8	7.3112	23.3	0.125*
CH_3COCH_3:CH_3OH	140	1346.1	7.4290	–	–
		1350.9	7.4025	–	–
		1364.4	7.3293	7.5	0.0404
CH_3COCH_3:H_2O:CO_2		1356.7	7.3710	–	–
		1367.3	7.3138	23.3	0.125*
CH_3COCH_3:H_2O:CH_4		1365.6	7.3228	21.8	
CH_3COCH_3:CH_3OH:CO		1345.6	7.4317	–	–
		1349.9	7.4078	–	–
		1364.4	7.3293	7.5	0.0404

Table B.4. Peak position and FWHM of the acetone CCC asymmetric deformation mode for pure acetone and mixtures with acetone ratio 1:5 and for temperatures ranging from 15 K to 140 K. See also Figs. 4. and 5.

Mixture	Temperature	Peak position		*FWHM*	
	(K)	(cm^{-1})	(μm)	(cm^{-1})	(μm)
CH_3COCH_3		1228.4	8.1404	12.8	0.0640
CH_3COCH_3:CO		1228.2	8.1420	9.5	0.0630
CH_3COCH_3:CO_2		1230.6	8.1261	9.4	0.0620
CH_3COCH_3:H_2O		1242.9	8.0457	17.3	0.112
CH_3COCH_3:CH_3OH	15	1226.0	8.1565	21.5	0.142*
		1238.1	8.0770	–	–
CH_3COCH_3:H_2O:CO_2		1240.5	8.0614	16.1	0.105
CH_3COCH_3:H_2O:CH_4		1242.4	8.0489	16.3	
CH_3COCH_3:CH_3OH:CO		1226.5	8.1532	7.8	0.052
		1238.6	8.0739	10.2	0.0662

Table B.4. continued.

Mixture	Temperature	Peak position		*FWHM*	
	(K)	(cm^{-1})	(μm)	(cm^{-1})	(μm)
$3COCH_3$		1228.4	8.1404	12.6	0.0836
CH_3COCH_3:CO		33 1229.9	8.1309	9.4	0.0624
CH_3COCH_3:CO_2		1230.6	8.1261	9.2	0.0606
CH_3COCH_3:H_2O		1239.5	8.0676	17.0	0.110
CH_3COCH_3:CH_3OH	30	1226.0	8.1565	21.4	0.141*
		1238.3	8.0755	–	–
CH_3COCH_3:H_2O:CO_2		1240.5	8.0614	15.7	0.102
CH_3COCH_3:H_2O:CH_4		1241.2	8.0567	16.2	
CH_3COCH_3:CH_3OH:CO		1226.7	8.1516	7.6	0.0506
		1238.8	8.0723	9.1	0.0594
CH_3COCH_3		1228.0	8.1436	11.8	0.0784
CH_3COCH_3:CO		–	–	–	–
CH_3COCH_3:CO_2		1230.4	8.1277	9.4	0.0620
CH_3COCH_3:H_2O		1239.5	8.0676	17.0	0.110*
CH_3COCH_3:CH_3OH	70	1226.0	8.1565	–	–
		1238.3	8.0755	21.6	0.142
CH_3COCH_3:H_2O:CO_2		1240.0	8.0645	14.8	0.0960
CH_3COCH_3:H_2O:CH_4		1239.0	8.071	14.7	
CH_3COCH_3:CH_3OH:CO		1226.5	8.1532	8.7	0.0577
		1238.6	8.0739		–
CH_3COCH_3		1227.5	8.1468	11.3	0.0750
CH_3COCH_3:CO		–	–	–	–
CH_3COCH_3:CO_2		1228.9	8.1373	10.5	0.0697
CH_3COCH_3:H_2O		1239.3	8.0692	16.7	0.108
CH_3COCH_3:CH_3OH	90	1225.8	8.1581	7.9	0.0528
		1237.8	8.0786	–	–
CH_3COCH_3:H_2O:CO_2		1239.0	8.0708	14.1	0.0918
CH_3COCH_3:H_2O:CH_4		1238.8	8.0723	13.6	
CH_3COCH_3:CH_3OH:CO		1226.3	8.1548	9.0	0.0598
		1237.8	8.0786	–	–
CH_3COCH_3		1233.0	8.1102	5.0	0.0327
CH_3COCH_3:CO		–	–	–	–
CH_3COCH_3:CO_2		1228.7	8.1389	11.0	0.0728
CH_3COCH_3:H_2O		1239.0	8.0708	16.5	0.107
CH_3COCH_3:CH_3OH	100	1225.5	8.1597	8.0	0.0532
		1237.6	8.0802	–	–
CH_3COCH_3:H_2O:CO_2		1238.6	8.0739	13.5	0.0876
CH_3COCH_3:H_2O:CH_4		1238.8	8.0723	12.9	
CH_3COCH_3:CH_3OH:CO		1226.0	8.1565	8.9	0.0593
		1235.2	8.0960	–	–
CH_3COCH_3		1232.8	8.1118	5.1	0.0337
CH_3COCH_3:CO		–	–	–	–
CH_3COCH_3:CO_2		–	–	–	–
CH_3COCH_3:H_2O		1238.8	8.0723	16.2	0.105
CH_3COCH_3:CH_3OH	110	1225.4	8.1606	7.7	0.0516
		1237.1	8.0833	–	–
CH_3COCH_3:H_2O:CO_2		1238.3	8.0755	12.8	0.0835
CH_3COCH_3:H_2O:CH_4		1239.0	8.071	12.4	
CH_3COCH_3:CH_3OH:CO		1224.6	8.1661	21.8	0.143
CH_3COCH_3		1232.5	8.1134	5.3	0.0347
CH_3COCH_3:CO		–	–	–	–
CH_3COCH_3:CO_2		–	–	–	–
CH_3COCH_3:H_2O		1238.8	8.0723	16.1	0.104
CH_3COCH_3:CH_3OH	120	1224.6	8.1661	–	–
		1234.9	8.0975	4.5	0.0294
CH_3COCH_3:H_2O:CO_2		1238.1	8.0770	12.4	0.0808
CH_3COCH_3:H_2O:CH_4		1238.2	8.0762	20.35	
CH_3COCH_3:CH_3OH:CO		1224.6	8.1661	23.9	0.157
CH_3COCH_3		1232.0	8.1166	5.4	0.0357
CH_3COCH_3:CO		–	–	–	–
CH_3COCH_3:CO_2		–	–	–	–
CH_3COCH_3:H_2O		1226.3	8.1548	–	–
		1247.9	8.0132	25.2	0.165*
CH_3COCH_3:CH_3OH	140	1233.7	8.1055	3.6	0.0238
CH_3COCH_3:H_2O:CO_2		1224.8	8.1645	–	–
		1236.1	8.0896	21.7	0.143*
CH_3COCH_3:H_2O:CH_4		1238	8.077	19.5	
CH_3COCH_3:CH_3OH:CO		1233.3	8.1086	3.8	0.0252

Table B.5. Peak position and FWHM of the acetone CO in-plane deformation mode for pure acetone and mixtures with acetone ratio 1:5 and for temperatures ranging from 15 K to 140 K. See also Figs. A.5 and A.6.

Mixture	Temperature	Peak position		*FWHM*	
	(K)	(cm^{-1})	(μm)	(cm^{-1})	(μm)
CH_3COCH_3		532.7	18.771	7.6	0.266
CH_3COCH_3:CO		532.0	18.796	4.4	0.155
CH_3COCH_3:CO_2		535.6	18.669	6.8	0.236
CH_3COCH_3:H_2O	15	547.0	18.283	17.5	0.588
CH_3COCH_3:CH_3OH		532.5	18.779	6.4	0.224
CH_3COCH_3:H_2O:CO_2		544.8	18.356	16.1	0.539
CH_3COCH_3:H_2O:CH_4		544.1	18.38	11.5	
CH_3COCH_3:CH_3OH:CO		532.0	18.796	4.9	0.174
CH_3COCH_3		532.7	18.771	7.5	0.264
CH_3COCH_3:CO		532.5	18.779	4.7	0.165
CH_3COCH_3:CO_2		535.6	18.669	6.5	0.226
CH_3COCH_3:H_2O		542.6	18.429	15.8	0.533
CH_3COCH_3:CH_3OH	30	532.0	18.796	6.2	0.219
CH_3COCH_3:H_2O:CO_2		544.6	18.364	16.0	0.536
CH_3COCH_3:H_2O:CH_4		545.3	18.78	11.6	
CH_3COCH_3:CH_3OH:CO		532.7	18.771	5.2	0.184
CH_3COCH_3		532.5	18.779	7.1	0.249
CH_3COCH_3:CO		–	–	–	–
CH_3COCH_3:CO_2		535.1	18.686	6.4	0.228
CH_3COCH_3:H_2O		542.6	18.429	15.8	0.533
CH_3COCH_3:CH_3OH	70	532.3	18.788	5.9	0.209
CH_3COCH_3:H_2O:CO_2		544.8	18.356	12.2	0.411
CH_3COCH_3:H_2O:CH_4		542.1	18.45	10.7	
CH_3COCH_3:CH_3OH:CO		532.5	18.779	5.5	0.192
CH_3COCH_3		532.3	18.788	6.8	0.240
CH_3COCH_3:CO		–	–	–	–
CH_3COCH_3:CO_2		533.7	18.737	6.0	0.213
CH_3COCH_3:H_2O		542.1	18.445	12.5	0.422
CH_3COCH_3:CH_3OH	90	531.8	18.805	5.2	0.185
CH_3COCH_3:H_2O:CO_2		541.9	18.454	10.3	0.347
CH_3COCH_3:H_2O:CH_4		542.1	18.45	10.4	
CH_3COCH_3:CH_3OH:CO		531.5	18.813	5.6	0.198
CH_3COCH_3		532.7	18.771	4.0	0.141
CH_3COCH_3:CO		–	–	–	–
CH_3COCH_3:CO_2		532.7	18.771	6.2	0.219
CH_3COCH_3:H_2O		542.1	18.445	11.6	0.392
CH_3COCH_3:CH_3OH	100	531.8	18.805	5.1	0.181
CH_3COCH_3:H_2O:CO_2		543.3	18.404	8.5	0.289
CH_3COCH_3:H_2O:CH_4		542.1	18.45	10.5	
CH_3COCH_3:CH_3OH:CO		532.5	18.779	5.5	0.194
CH_3COCH_3		532.5	18.779	4.1	0.141
CH_3COCH_3:CO		–	–	–	–
CH_3COCH_3:CO_2		–	–	–	–
CH_3COCH_3:H_2O	110	542.1	18.445	9.7	0.330
CH_3COCH_3:CH_3OH		531.5	18.813	4.8	0.171
CH_3COCH_3:H_2O:CO_2		541.9	18.454	7.5	0.254
CH_3COCH_3:H_2O:CH_4		542.4	18.44	10.1	
CH_3COCH_3:CH_3OH:CO		533.0	18.762	3.3	0.114
CH_3COCH_3		532.3	18.788	4.1	0.143
CH_3COCH_3:CO		–	–	–	–
CH_3COCH_3:CO_2		–	–	–	–
CH_3COCH_3:H_2O	120	542.1	18.445	8.7	0.296
CH_3COCH_3:CH_3OH		533.9	18.728	3.7	0.129
CH_3COCH_3:H_2O:CO_2		541.9	18.454	5.6	0.189
CH_3COCH_3:H_2O:CH_4		531.5	18.81	7.0	
CH_3COCH_3:CH_3OH:CO		533.0	18.762	3.1	0.110
CH_3COCH_3		531.5	18.813	4.2	0.147
CH_3COCH_3:CO		–	–	–	–
CH_3COCH_3:CO_2		–	–	–	–
CH_3COCH_3:H_2O		541.9	18.454	–	–
	140	529.6	18.882	–	–
CH_3COCH_3:CH_3OH		533.0	18.762	2.7	0.097
CH_3COCH_3:H_2O:CO_2		–	–	–	–
CH_3COCH_3:H_2O:CH_4		531.1	18.83	6.3	
CH_3COCH_3:CH_3OH:CO		532.7	18.77	3.4	0.129

Table B.6. Peak position and FWHM of the acetone CO-stretch mode for pure acetone and mixtures with acetone ratio 1:20 and for temperatures ranging from 15 K to 140 K. See also Figs. A.7 and A.8.

Mixture	Temperature	Peak position		*FWHM*	
	(K)	(cm^{-1})	(μm)	(cm^{-1})	(μm)
CH_3COCH_3		1710.3	5.8469	18.7	0.0640
CH_3COCH_3:CO		1717.3	5.8231	6.8	0.0232
CH_3COCH_3:CO_2		1710.6	5.8461	11.5	0.0392
CH_3COCH_3:H_2O		1696.8	5.8934	23.5	0.0813
CH_3COCH_3:CH_3OH	15	1699.5	5.8842	–	–
		1708.9	5.8518	21.2	0.0731*
CH_3COCH_3:H_2O:CO_2		1695.6	5.8976	21.4	0.0745
CH_3COCH_3:H_2O:CH_4		1697.5	5.9810	17.1	
CH_3COCH_3:CH_3OH:CO		1700.2	5.8817	20.4	0.0704*
		1711.1	5.8444	–	–
CH_3COCH_3		1709.8	5.8485	18.7	0.0640
CH_3COCH_3:CO		1717.3	5.8231	9.7	0.0330
CH_3COCH_3:CO_2		1710.6	5.8461	11.3	0.0384
CH_3COCH_3:H_2O		1696.8	5.8934	23.5	0.0816
CH_3COCH_3:CH_3OH	30	1699.0	5.8859	–	–
		1709.6	5.8494	21.5	0.0742*
CH_3COCH_3:H_2O:CO_2		1695.8	5.8968	21.0	0.0728
CH_3COCH_3:H_2O:CH_4		1697.5	5.8910	16.9	
CH_3COCH_3:CH_3OH:CO		1699.9	5.8825	–	–
		1711.5	5.8428	12.0	0.0416
CH_3COCH_3		1708.9	5.8518	18.3	0.0628
CH_3COCH_3:CO		–	–	–	–
CH_3COCH_3:CO_2		1716.6	5.8255	11.3	0.0384
CH_3COCH_3:H_2O		1696.8	5.8934	24.6	0.0853*
CH_3COCH_3:CH_3OH	70	1698.5	5.8876		–
		1710.3	5.8469	20.0	0.0680*
CH_3COCH_3:H_2O:CO_2		1695.1	5.8993	19.7	0.0684
CH_3COCH_3:H_2O:CH_4		1695.4	5.8983	20.7	
CH_3COCH_3:CH_3OH:CO		1698.3	5.8884	–	–
		1710.8	5.8452	10.6	0.0362
CH_3COCH_3		1708.6	5.8527	17.8	0.0611
CH_3COCH_3:CO		–	–	–	–
CH_3COCH_3:CO_2		1716.3	5.8264	12.4	0.0422
CH_3COCH_3:H_2O		1696.8	5.8934	25.7	0.0891
CH_3COCH_3:CH_3OH	90	1698.0	5.8892	–	–
		1710.6	5.8461	9.0	0.0308
CH_3COCH_3:H_2O:CO_2		1695.1	5.8993	20.0	0.0697
CH_3COCH_3:H_2O:CH_4		1695.1	5.8994	21.0	
CH_3COCH_3:CH_3OH:CO		1697.5	5.8909	–	–
		1710.1	5.8477	10.7	0.0367
CH_3COCH_3		1697.5	5.8909	–	–
		1706.7	5.8593	–	–
		1713.9	5.8346	13.5	0.0463*
CH_3COCH_3:CO		–	–	–	–
CH_3COCH_3:CO_2	100	1706.9	5.8585	11.4	0.0391*
		1713.7	5.8354	–	–
CH_3COCH_3:H_2O		1696.8	5.8934	25.8	0.0895*
CH_3COCH_3:CH_3OH		1698.0	5.8892	–	–
		1710.6	5.8461	9.0	0.0306*
CH_3COCH_3:H_2O:CO_2		1700.9	5.8792	22.4	0.0775
CH_3COCH_3:H_2O:CH_4		1695.4	5.8983	21.6	
CH_3COCH_3:CH_3OH:CO		1698.0	5.8892	–	–
		1710.3	5.8469	10.7	0.0367
CH_3COCH_3		1697.8	5.8901	–	–
		1706.9	5.8585	–	–
		1713.9	5.8346	13.5	0.0463*
CH_3COCH_3:CO		–	–	–	–
CH_3COCH_3:CO_2		–	–	–	–
CH_3COCH_3:H_2O	110	1699.0	5.8859	25.9	0.0898
CH_3COCH_3:CH_3OH		1699.2	5.8851	–	–
		1710.6	5.8461	9.8	0.0335
CH_3COCH_3:H_2O:CO_2		1701.4	5.8775	22.6	0.0783
CH_3COCH_3:H_2O:CH_4		1695.1	5.8994	22.1	
CH_3COCH_3:CH_3OH:CO		1698.3	5.8884	–	–
		1707.9	5.8551	12.3	0.0420*
		1714.2	5.8337	–	–

Table B.6. continued.

Mixture	Temperature	Peak position		*FWHM*	
	(K)	(cm^{-1})	(μm)	(cm^{-1})	(μm)
CH_3COCH_3		1698.0	5.8892	–	–
		1706.9	5.8585	–	–
		1713.9	5.8346	13.5	0.0460*
CH_3COCH_3:CO		–	–	–	–
CH_3COCH_3:CO_2		–	–	–	–
CH_3COCH_3:H_2O		1703.3	5.8709	25.9	0.0895
CH_3COCH_3:CH_3OH	120	1707.4	5.8568	19.5	0.0669
CH_3COCH_3:H_2O:CO_2		1703.6	5.8701	21.9	0.0759
CH_3COCH_3:H_2O:CH_4		1697.8	5.8900	23.2	
CH_3COCH_3:CH_3OH:CO		1698.0	5.8892	–	–
		1707.9	5.8551	11.5	0.0393*
		1714.4	5.8329	–	–
CH_3COCH_3		1698.0	5.8892	–	–
		1706.9	5.8585	–	–
		1713.7	5.8354	13.3	0.0453*
CH_3COCH_3:CO		–	–	–	–
CH_3COCH_3:CO_2		–	–	–	–
CH_3COCH_3:H_2O	140	1703.3	5.8709	25.4	0.0880
CH_3COCH_3:CH_3OH		1697.8	5.8901	–	–
		1708.1	5.8543	5.4	0.0187
		1714.2	5.8337	–	–
CH_3COCH_3:H_2O:CO_2		1705.7	5.8626	32.1	0.110
CH_3COCH_3:H_2O:CH_4		1708.6	5.8527	30.3	
CH_3COCH_3:CH_3OH:CO		–	–	–	–
CH_3COCH_3		–	–	–	–
CH_3COCH_3:CO		–	–	–	–
CH_3COCH_3:CO_2		–	–	–	–
CH_3COCH_3:H_2O	160	1703.1	5.8717	38.8	0.134
CH_3COCH_3:CH_3OH		–	–	–	–
CH_3COCH_3:H_2O:CO_2		–	–	–	–
CH_3COCH_3:H_2O:CH_4		–	–	–	–
CH_3COCH_3:CH_3OH:CO		–	–	–	–

Table B.7. Peak position and FWHM of the acetone CH_3 asymmetric deformation mode for pure acetone and mixtures with acetone ratio 1:20 and for temperatures ranging from 15 K to 140 K. See also Figs. A.9 and A.10.

Mixture	Temperature	Peak position		*FWHM*	
	(K)	(cm^{-1})	(μm)	(cm^{-1})	(μm)
CH_3COCH_3		1417.9	7.0527	40.9	0.199*
		1441.0	6.9394	–	–
CH_3COCH_3:CO		1416.9	7.0575	9.5	0.0475
		1435.0	6.9685	17.3	0.0885*
		1443.7	6.9267	–	–
CH_3COCH_3:CO_2	15	1420.3	7.0407	9.5	0.0469
		1445.4	6.9186	–	–
CH_3COCH_3:H_2O		1422.0	7.0323	14.8	0.0730
		1445.3	6.9192	–	–
CH_3COCH_3:H_2O :CO_2		1422.5	7.0299	12.7	0.0624
		1444.4	6.9232	–	–
CH_3COCH_3:H_2O:CH_4		1422.7		12.1	
		1443.0			
CH_3COCH_3		1417.9	7.0527	40.9	0.199*
		1441.3	6.9382	–	–
CH_3COCH_3:CO		1417.4	7.0551	10.6	0.0527
		1436.7	6.9604	17.1	0.0912
CH_3COCH_3:CO_2	30	1420.6	7.0395	11.2	0.0556
		1444.9	6.9209	–	–
CH_3COCH_3:H_2O		1421.8	7.0335	14.5	0.0716
		1442.0	6.9348	–	–
CH_3COCH_3:H_2O :CO_2		1422.2	7.0311	12.9	0.0635
		1444.4	6.9232	–	–
CH_3COCH_3:H_2O:CH_4		1422.7	7.0289	12.0	
		1443.2	6.929		

Table B.7. continued.

Mixture	Temperature	Peak position		*FWHM*	
	(K)	(cm^{-1})	(μm)	(cm^{-1})	(μm)
CH_3COCH_3		1418.1	7.0515	39.6	0.193*
		1441.0	6.9394	–	–
CH_3COCH_3:CO		–	–	–	–
CH_3COCH_3:CO_2		1420.3	7.0407	37.5	0.183*
		1439.4	6.9475	–	–
CH_3COCH_3:H_2O	70	1421.5	7.0347	14.0	0.0693
		1439.9	6.9450	–	–
CH_3COCH_3:H_2O :CO_2		1422.2	7.0311	–	–
		1442.3	6.9336	12.2	0.0601
CH_3COCH_3:H_2O:CH_4		1423.2	7.0264	13.8	
		1441.2	6.9387		
CH_3COCH_3		1418.1	7.0515	38.7	0.189*
		1440.8	6.9406	–	–
CH_3COCH_3:CO		–	–	–	–
CH_3COCH_3:CO_2		1419.8	7.0431	35.5	0.173*
		1439.6	6.9464	–	–
CH_3COCH_3:H_2O	90	1421.5	7.0347	13.9	0.0685
		1439.5	6.9467	–	–
CH_3COCH_3:H_2O :CO_2		1422.2	7.0311	12.2	0.0602
		1441.0	6.9359	–	–
CH_3COCH_3:H_2O:CH_4		1423.4	7.0254	13.9	
		1443.0	6.93		
CH_3COCH_3		1401.8	7.1339	–	–
		1417.4	7.0551	10.8	0.0538
CH_3COCH_3:CO		–	–	–	–
CH_3COCH_3:CO_2		1417.4	7.0551	13.7	0.0682
		1437.2	6.9580	–	–
CH_3COCH_3:H_2O	100	1421.8	7.0335	14.1	0.0695
CH_3COCH_3:H_2O :CO_2		1422.0	7.0323	14.9	0.0735
		1439.6	6.9464	–	–
CH_3COCH_3:H_2O:CH_4		1423.4	7.0254	14.0	
		1441.0	6.9396		
CH_3COCH_3		1402.2	7.1315	–	–
		1417.7	7.0539	11.5	0.0569
		1438.6	6.9510	–	–
CH_3COCH_3:CO		–	–	–	–
CH_3COCH_3:CO_2		–	–	–	–
CH_3COCH_3:H_2O	110	1421.8	7.0335	14.7	0.0727
CH_3COCH_3:H_2O :CO_2		1422.0	7.0323	–	–
		1439.6	6.9464	14.8	0.0731
CH_3COCH_3:H_2O:CH_4		1423.4	7.0254	14.5	
		1441.0	6.9396		
CH_3COCH_3		1402.5	7.1302	–	–
		1417.9	7.0527	12.1	0.0599
CH_3COCH_3:CO		–	–	–	–
CH_3COCH_3:CO_2		–	–	–	–
CH_3COCH_3:H_2O	120	1421.8	7.0335	14.5	0.0715
CH_3COCH_3:H_2O :CO_2		1422.0	7.0323	15.2	0.0752
		143.7	6.9557	–	–
CH_3COCH_3:H_2O:CH_4		1423.4	7.0254	14.1	
		1438.9	6.9498		
CH_3COCH_3		1404.9	7.1180	–	–
		1417.7	7.0539	12.2	0.0607
		1439.8	6.9452	–	–
CH_3COCH_3:CO		–	–	–	–
CH_3COCH_3:CO_2		–	–	–	–
CH_3COCH_3:H_2O	140	1421.8	7.0335	16.4	0.0812
CH_3COCH_3:H_2O:CO_2		1417.4	7.0551	27.1	0.133*
		1437.5	6.9566	–	–
CH_3COCH_3:H_2O:CH_4		1421.3	7.0358	29.5	
		1438.6	6.9512		
CH_3COCH_3		–	–	–	–
CH_3COCH_3:CO		–	–	–	–
CH_3COCH_3:CO_2	160	–	–	–	–
CH_3COCH_3:H_2O		1422.0	7.0323	25.2	0.124
CH_3COCH_3:H_2O :CO_2		–	–	–	–

Table B.8. Peak position and FWHM of the acetone CH_3 symmetric deformation mode for pure acetone and mixtures with acetone ratio 1:20 and for temperatures ranging from 15 K to 140 K. See also Figs. A.11 and A.12.

Mixture	Temperature	Peak position		*FWHM*	
	(K)	(cm^{-1})	(μm)	(cm^{-1})	(μm)
CH_3COCH_3		1363.4	7.3345	19.2	0.0640
CH_3COCH_3:CO		1353.3	7.3893	6.1	0.0332
		1363.9	7.3319	5.7	0.0308
CH_3COCH_3:CO_2		1356.9	7.3696	6.6	0.0358
		1367.5	7.3125	6.2	0.0333
CH_3COCH_3:H_2O	15	1358.1	7.3631	–	–
		1371.9	7.2894	13.2	0.180
CH_3COCH_3:CH_3OH		1367.3	7.3138	16.3	0.0870*
CH_3COCH_3:H_2O:CO_2		1359.3	7.3566	–	–
		1372.6	7.2855	11.1	0.0588
CH_3COCH_3:H_2O:CH_4		1359.8	7.354	10.7	
		1373.1	7.2828	10.9	
CH_3COCH_3:CH_3OH:CO		1356.7	7.3710	–	–
		1370.4	7.2971	14.6	0.0779
CH_3COCH_3		1363.2	7.3358	19.7	0.106
CH_3COCH_3:CO		1352.8	7.3920	8.1	0.0408
		1363.9	7.3319	7.6	0.0440
CH_3COCH_3:CO_2		1356.7	7.3710	–	–
		1367.5	7.3125	6.6	0.0353
CH_3COCH_3:H_2O	30	1358.1	7.3631	–	–
		1371.6	7.2906	13.5	0.0717
CH_3COCH_3:CH_3OH		1366.8	7.3164	16.6	0.0888
CH_3COCH_3:H_2O:CO_2		1359.1	7.3579	–	–
		1372.3	7.2868	11.3	0.0600
CH_3COCH_3:H_2O:CH_4		1360.3	7.3513	10.5	
		1372.8	7.2843	10.7	
CH_3COCH_3:CH_3OH:CO		1356.4	7.3723	–	–
		1370.7	7.2958	14.0	0.0745
CH_3COCH_3		1363.2	7.3358	20.8	0.112
CH_3COCH_3:CO		–	–	–	–
CH_3COCH_3:CO_2		1365.1	7.3254	16.5	0.0888
CH_3COCH_3:H_2O		1357.2	7.3683	–	–
		1369.9	7.2996	15.5	0.0826
CH_3COCH_3:CH_3OH	70	1364.4	7.3293	16.9	0.0909
CH_3COCH_3:H_2O:CO_2		1359.1	7.3579	–	–
		1372.1	7.2881	11.7	0.0623
CH_3COCH_3:H_2O:CH_4		1359.6	7.3551	10.5	
		1372.8	7.284	13.3	
CH_3COCH_3:CH_3OH:CO		1354.3	7.3841	–	–
		1364.1	7.3306	11.6	0.0623
CH_3COCH_3		1363.2	7.3358	21.0	0.113
CH_3COCH_3:CO		–	–	–	–
CH_3COCH_3:CO_2		1365.1	7.3254	16.5	0.0892
CH_3COCH_3:H_2O		1356.9	7.3696	–	–
		1369.7	7.3009	22.4	0.120*
CH_3COCH_3:CH_3OH	90	1363.7	7.3332	15.9	0.0852
CH_3COCH_3:H_2O:CO_2		1359.1	7.3579	–	–
		1371.9	7.2894	12.3	0.0656
CH_3COCH_3:H_2O:CH_4		1359.8	7.354	10.3	
		1372.8	7.284	14.1	
CH_3COCH_3:CH_3OH:CO		1354.3	7.3841	–	–
		1363.7	7.3332	12.0	0.0644
CH_3COCH_3		1345.3	7.4330	7.7	0.0424*
		1349.2	7.4118	–	–
		1361.3	7.3462	8.8	0.0472
CH_3COCH_3:CO		–	–	–	–
CH_3COCH_3:CO_2		1351.1	7.4012	–	–
		1369.7	7.3009	14.0	0.0750
CH_3COCH_3:H_2O	100	1356.9	7.3696	–	–
		1369.7	7.3009	22.5	0.120
CH_3COCH_3:CH_3OH		1363.7	7.3332	15.5	0.0834*
CH_3COCH_3:H_2O:CO_2		1358.4	7.3618	–	–
		1371.1	7.2932	22.4	0.1200

Table B.8. continued.

Mixture	Temperature	Peak position		*FWHM*	
	(K)	(cm^{-1})	(μm)	(cm^{-1})	(μm)
CH_3COCH_3:H_2O:CH_4		1360.3	7.351	10.3	
		1372.8	7.284	14.4	
CH_3COCH_3:CH_3OH:CO		1354.5	7.3831	–	–
		1363.7	7.3332	12.5	0.0674
CH_3COCH_3		1345.6	7.4317	7.5	0.0413*
		1349.2	7.4118	–	–
		1361.0	7.3475	8.7	0.0471
CH_3COCH_3:CO		–	–	–	–
CH_3COCH_3:CO_2		–	–	–	–
CH_3COCH_3:H_2O	110	1356.9	7.3696	–	–
		1369.5	7.3022	22.6	0.121*
CH_3COCH_3:CH_3OH		1363.4	7.3345	19.9	0.107
CH_3COCH_3:H_2O:CO_2		1358.1	7.3631	–	–
		1369.9	7.2996	22.2	0.119*
CH_3COCH_3:H_2O:CH_4		1359.8	7.354	9.5	
		1372.8	7.284	15.0	
CH_3COCH_3:CH_3OH:CO		1349.9	7.4078	–	–
		1363.7	7.3332	12.1	0.0650
CH_3COCH_3		1346.1	7.4290	7.3	0.0404*
		1349.4	7.4105	–	–
		1360.8	7.3488	8.7	0.0470
CH_3COCH_3:CO		–	–	–	–
CH_3COCH_3:CO_2		–	–	–	–
CH_3COCH_3:H_2O	120	1356.7	7.3710	–	–
		1369.5	7.3022	22.6	0.121*
CH_3COCH_3:CH_3OH		1363.7	7.3332	24.6	0.133*
CH_3COCH_3:H_2O:CO_2		1356.9	7.3696	–	–
		1369.9	7.2996	22.6	0.121*
CH_3COCH_3:H_2O:CH_4		1372.6	7.285	15.6	
		1359.8	7.354	8.7	
CH_3COCH_3:CH_3OH:CO		1345.1	7.4344	–	–
		1349.7	7.4091	–	–
		1363.7	7.3332	10.9	0.0583
CH_3COCH_3		1346.6	7.4264	–	–
		1350.9	7.4025	–	–
		1361.7	7.3436	9.3	0.0499
CH_3COCH_3:CO		–	–	–	–
CH_3COCH_3:CO_2		–	–	–	–
CH_3COCH_3:H_2O		1356.7	7.3710	–	–
		1369.2	7.3035	23.1	0.124*
CH_3COCH_3:CH_3OH	140	1363.7	7.3332	14.0	0.0753
CH_3COCH_3:H_2O:CO_2		1356.4	7.3723	–	–
		1364.9	7.3267	20.5	0.110*
CH_3COCH_3:H_2O:CH_4		1366.1	7.320	–	
CH_3COCH_3:CH_3OH:CO		–	–	–	–
CH_3COCH_3		–	–	–	–
CH_3COCH_3:CO		–	–	–	–
CH_3COCH_3:CO_2		–	–	–	–
CH_3COCH_3:H_2O	160	1357.5	7.3666	–	–
		1367.0	7.3151	23.3	0.125
CH_3COCH_3:CH_3OH		–	–	–	–
CH_3COCH_3:H_2O:CO_2		–	–	–	–
CH_3COCH_3:H_2O:CH_4			–	–	–
CH_3COCH_3:CH_3OH:CO		–	–	–	–

Table B.9. Peak position and FWHM of the acetone CCC asymmetric deformation mode for pure acetone and mixtures with acetone ratio 1:20 and for temperatures ranging from 15 K to 140 K. See also Figs. A.13 and A.14.

Mixture	Temperature	Peak position		*FWHM*	
	(K)	(cm^{-1})	(μm)	(cm^{-1})	(μm)
CH_3COCH_3		1228.4	8.1404	12.8	0.0640
CH_3COCH_3:CO		1224.1	8.1693	9.6	0.0641*
		1231.3	8.1216	–	–
CH_3COCH_3:CO_2		1230.8	8.1245	7.6	0.0502
CH_3COCH_3:H_2O	15	1244.6	8.0348	14.6	0.0947

Table B.9. continued.

Mixture	Temperature	Peak position		*FWHM*	
	(K)	(cm^{-1})	(μm)	(cm^{-1})	(μm)
CH_3COCH_3:CH_3OH		1225.5	8.1597	8.3	0.0554
		1238.1	8.0770	9.7	0.0635
CH_3COCH_3:H_2O:CO_2		1244.6	8.0348	14.2	0.0919
CH_3COCH_3:H_2O:CH_4		1244.6	8.035	12.1	
CH_3COCH_3:CH_3OH:CO		1226.3	8.1548	6.3	0.0419
		1239.3	8.0692	9.0	0.0588
CH_3COCH_3		1228.4	8.1404	12.6	0.0836
CH_3COCH_3:CO		1228.7	8.1389	10.6	0.0706
CH_3COCH_3:CO_2		1230.8	8.1245	8.0	0.0529
CH_3COCH_3:H_2O	30	1244.6	8.0348	14.8	0.0956
CH_3COCH_3:CH_3OH		1225.3	8.1613	7.6	0.0507
		1238.3	8.075	9.2	0.06
CH_3COCH_3:H_2O:CO_2		1244.6	8.035	14.2	0.092
CH_3COCH_3:H_2O:CH_4		1244.3	8.037	12.0	
CH_3COCH_3:CH_3OH:CO		1226.3	8.1548	6.0	0.0400
		1239.5	8.0676	7.7	0.0500
CH_3COCH_3		1228.0	8.14	11.8	0.078
CH_3COCH_3:CO		–	–	–	–
CH_3COCH_3:CO_2		1227.2	8.1484	11.7	0.0778
CH_3COCH_3:H_2O	70	1244.3	8.0364	16.4	0.1062
CH_3COCH_3:CH_3OH		1225.3	8.1613	6.8	0.0450
		1238.1	8.0770	8.1	0.0527
CH_3COCH_3:H_2O:CO_2		1244.6	8.0348	13.5	0.0870
CH_3COCH_3:H_2O:CH_4		1245.5	8.029	14.5	
CH_3COCH_3:CH_3OH:CO		1227.23	8.1484	7.25	–
		1239.5	8.0677	8.43	0.048
CH_3COCH_3		1227.5	8.1468	11.3	0.0750
CH_3COCH_3:CO		–	–	–	–
CH_3COCH_3:CO_2		1227.2	8.1484	11.0	0.0729
CH_3COCH_3:H_2O		1237.7	8.0793	–	–
		1244.3	8.0364	17.0	0.1100
CH_3COCH_3:CH_3OH	90	1225.1	8.1629	6.6	0.0440
		1238.1	8.0770	8.0	0.0521
CH_3COCH_3:H_2O:CO_2		1244.6	8.0348	14.3	0.0923
CH_3COCH_3:H_2O:CH_4		1245.5	8.029	14.7	
CH_3COCH_3:CH_3OH:CO		1227.0	8.1499	7.41	–
		1239.0	8.0710	7.4	0.049
CH_3COCH_3		1233.0	8.1102	5.0	0.0327
CH_3COCH_3:CO		–	–	–	–
CH_3COCH_3:CO_2		1226.7	8.1516	–	–
		1236.9	8.0849	4.3	0.0282
CH_3COCH_3:H_2O		1237.2	8.0827	–	–
		1244.3	8.0364	17.1	0.111
CH_3COCH_3:CH_3OH	100	1225.1	8.1629	6.6	0.0437
		1237.8	8.0786	8.0	0.0524
CH_3COCH_3:H_2O:CO_2		1241.9	8.0520	16.1	0.1042
CH_3COCH_3:H_2O:CH_4		1245.5	8.029	15.0	
CH_3COCH_3:CH_3OH:CO		1226.5	8.1533	7.32	0.0490
		1239.0	8.0710	8.95	–
CH_3COCH_3		1232.8	8.1118	5.1	0.0337
CH_3COCH_3:CO		–	–	–	–
CH_3COCH_3:CO_2		–	–	–	–
CH_3COCH_3:H_2O	110	1237.6	8.0803	–	–
		1237.6	8.0802	17.3	0.112
CH_3COCH_3:CH_3OH		1224.8	8.1645	6.6	0.0438
		1236.6	8.0865	9.0	0.0591
CH_3COCH_3:H_2O:CO_2		1239.5	8.0676	16.3	0.105
CH_3COCH_3:H_2O:CH_4		1245.3	8.030	15.5	
CH_3COCH_3:CH_3OH:CO		1226.3	8.1549	7.38	–
		1234.9	8.0978	5.34	0.0352
CH_3COCH_3		1232.5	8.1134	5.3	0.0347
CH_3COCH_3:CO		–	–	–	–
CH_3COCH_3:CO_2		–	–	–	–
CH_3COCH_3:H_2O	120	1237.4	8.0818	–	–
		1244.3	8.0364	17.1	0.111

Table B.9. continued.

Mixture	Temperature	Peak position		*FWHM*	
	(K)	(cm^{-1})	(μm)	(cm^{-1})	(μm)
CH_3COCH_3:CH_3OH		1225.3	8.1613	19.3	0.127*
		1233.7	8.1055	–	–
CH_3COCH_3:H_2O:CO_2		1238.1	8.0770	16.4	0.107
CH_3COCH_3:H_2O:CH_4		1245.1	8.031	16.3	
CH_3COCH_3:CH_3OH:CO		1226.3	8.1548	5.6	–
		1234.7	8.0991	4.5	0.0297
CH_3COCH_3		1232.0	8.1166	5.4	0.0357
CH_3COCH_3:CO		–	–	–	–
CH_3COCH_3:CO_2		–	–	–	–
CH_3COCH_3:H_2O	140	1237.4	8.0818	–	–
		1244.3	8.0364	17.2	0.112
CH_3COCH_3:CH_3OH		1233.5	8.1070	3.6	0.0235
CH_3COCH_3:H_2O:CO_2		–	8.	–	–
		–	–	-	–
CH_3COCH_3:H_2O:CH_4		1225.8	8.158	7.1	
CH_3COCH_3:CH_3OH:CO		–	–	–	–
CH_3COCH_3		–	–	–	–
CH_3COCH_3:CO		–	–	–	–
CH_3COCH_3:CO_2		–	–	–	–
CH_3COCH_3:H_2O	160	1224.6	8.1661	–	–
		1235.7	8.0928	24.9	0.163
CH_3COCH_3:CH_3OH		–	–	–	–
CH_3COCH_3:H_2O:CO_2		–	–	–	–
CH_3COCH_3:H_2O:CH_4		–	–	–	–
CH_3COCH_3:CH_3OH:CO		–	–	–	–

Table B.10. Peak position and FWHM of the acetone CO in-plane deformation mode for pure acetone and mixtures with acetone ratio 1:20 and for temperatures ranging from 15 K to 120 K. See also Figs. A.15 and A.16.

Mixture	Temperature	Peak position		*FWHM*	
	(K)	(cm^{-1})	(μm)	(cm^{-1})	(μm)
CH_3COCH_3		532.7	18.77	7.6	0.266
CH_3COCH_3:CO		531.8	18.80	4.2	0.147
CH_3COCH_3:CO_2		536.1	18.65	7.4	0.257
CH_3COCH_3:H_2O	15	–	–	–	–
CH_3COCH_3:CH_3OH		–	–	–	–
CH_3COCH_3:H_2O:CO_2		–	–	–	–
CH_3COCH_3:H_2O:CH_4		546.0	18.31	9.5	
CH_3COCH_3:CH_3OH:CO		–	–	–	–
CH_3COCH_3		532.7	18.771	7.5	0.264
CH_3COCH_3:CO		532.5	18.779	4.7	0.165
CH_3COCH_3:CO_2		536.1	18.653	6.9	0.238
CH_3COCH_3:H_2O	30	–	–	–	–
CH_3COCH_3:CH_3OH		–	–	–	–
CH_3COCH_3:H_2O:CO_2		–	–	–	–
CH_3COCH_3:H_2O:CH_4		545.8	18.32	7.9	
CH_3COCH_3:CH_3OH:CO		–	–	–	–
CH_3COCH_3		532.5	18.779	7.1	0.249
CH_3COCH_3:CO		–	–	–	–
CH_3COCH_3:CO_2		533.5	18.745	5.5	0.194
CH_3COCH_3:H_2O	70	–	–	–	–
CH_3COCH_3:CH_3OH		–	–	–	–
CH_3COCH_3:H_2O:CO_2		–	–	–	–
CH_3COCH_3:H_2O:CH_4		545.8	18.32	4.0	
CH_3COCH_3:CH_3OH:CO		532.3	18.788	4.4	0.154
CH_3COCH_3		532.3	18.788	6.8	0.240
CH_3COCH_3:CO		–	–	–	–
CH_3COCH_3:CO_2		532.5	18.779	7.3	0.257
CH_3COCH_3:H_2O	90	–	–	–	–
CH_3COCH_3:CH_3OH		–	–	–	–
CH_3COCH_3:H_2O:CO_2		–	–	–	–
CH_3COCH_3:H_2O:CH_4		545.8	18.32	4.6	
CH_3COCH_3:CH_3OH:CO		532.3	18.788	4.7	0.167

Notes. For higher temperatures this band is not visible.

Table B.10. continued.

Mixture	Temperature	Peak position		*FWHM*	
	(K)	(cm^{-1})	(μm)	(cm^{-1})	(μm)
CH_3COCH_3		532.7	18.771	4.0	0.141
CH_3COCH_3:CO		–	–	–	–
CH_3COCH_3:CO_2		–	–	–	–
CH_3COCH_3:H_2O	100	–	–	–	–
CH_3COCH_3:CH_3OH		–	–	–	–
CH_3COCH_3:H_2O:CO_2		–	–	–	–
CH_3COCH_3:H_2O:CH_4		546.0	18.31	5.0	
CH_3COCH_3:CH_3OH:CO		532.0	18.796	4.6	0.162
CH_3COCH_3		532.5	18.779	4.1	0.141
CH_3COCH_3:CO		–	–	–	–
CH_3COCH_3:CO_2		–	–	–	–
CH_3COCH_3:H_2O	110	–	–	–	–
CH_3COCH_3:CH_3OH		–	–	–	–
CH_3COCH_3:H_2O:CO_2		–	–	–	–
CH_3COCH_3:H_2O:CH_4		546.0	18.31	4.4	
CH_3COCH_3:CH_3OH:CO		532.5	18.779	4.1	0.146
CH_3COCH_3		532.3	18.788	4.1	0.143
CH_3COCH_3:CO		–	–	–	–
CH_3COCH_3:CO_2		–	–	–	–
CH_3COCH_3:H_2O	120	–	–	–	–
CH_3COCH_3:CH_3OH		–	–	–	–
CH_3COCH_3:H_2O:CO_2		–	–	–	–
CH_3COCH_3:H_2O:CH_4		546.0	18.31	6.7	
CH_3COCH_3:CH_3OH:CO		532.5	18.779	2.9	0.103

Appendix C: Integrated absorbance values

In this section, the integrated absorbance of the analyzed acetone bands is presented in tables. The tables contain the integrated absorbance of the acetone bands normalized in relation to the C=O stretch mode of the respective mixture at 15 K.

All the measurements are taken from baseline-corrected spectra and for the C=O stretch band of acetone, water subtraction is also performed, since the O–H bending mode of water (around 1667 cm^{-1}) overlaps with this mode. For modes that present two or more overlapping components, the values listed below refer to the absorbance integrated over all the components (Tables C.1–C.15).

Table C.1. Integrated absorbance ratios of selected transitions in pure acetone ice.

Temperature (K)	C=O stretch (5.847 μm)	CH_3 assym. deformation (7.053 μm)	CH_3 symm. deformation (7.335 μm)	CCC asymm. stretch (8.141 μm)	CO in-plane deformation (18.77 μm)
15	1.00	0.40	0.53	0.27	0.08
30	1.00	0.40	0.53	0.27	0.08
70	1.01	0.39	0.52	0.28	0.08
90	1.02	0.38	0.52	0.28	0.07
100	0.89	0.31	0.62	0.30	0.09
110	0.90	0.31	0.61	0.30	0.09
120	0.91	0.30	0.61	0.30	0.09
140	0.79	0.26	0.49	0.25	0.07

Table C.2. Integrated absorbance ratios of selected transitions in CH_3COCH_3:H_2O(1:5).

Temperature (K)	C=O stretch (5.847 μm)	CH_3 assym. deformation (7.053 μm)	CH_3 symm. deformation (7.335 μm)	CCC asymm. stretch (8.141 μm)	CO in-plane deformation (18.77 μm)
15	1.00	0.33	0.44	0.19	0.060
30	1.04	0.33	0.45	0.20	0.059
70	1.03	0.31	0.44	0.19	0.055
90	1.02	0.30	0.43	0.19	0.044
100	1.02	0.29	0.43	0.19	–
110	1.02	0.29	0.42	0.18	–
120	1.01	0.27	0.42	0.19	–
140	0.86	0.24	0.40	0.20	–

Table C.3. Integrated absorbance ratios of selected transitions in CH_3COCH_3:CO_2(1:5).

Temperature (K)	C=O stretch (5.847 μm)	CH_3 assym. deformation (7.053 μm)	CH_3 symm. deformation (7.335 μm)	CCC asymm. stretch (8.141 μm)	CO in-plane deformation (18.77 μm)
15	1.00	0.37	0.56	0.28	0.087
30	1.01	0.37	0.56	0.28	0.084
70	1.05	0.38	0.57	0.30	0.067
90	1.00	0.32	0.51	0.27	0.044
100	1.00	0.30	0.48	0.25	0.044

Table C.4. Integrated absorbance ratios of selected transitions in CH_3COCH_3:CO(1:5).

Temperature (K)	C=O stretch (5.847 μm)	CH_3 assym. deformation (7.053 μm)	CH_3 symm. deformation (7.335 μm)	CCC asymm. stretch (8.141 μm)	CO in-plane deformation (18.77 μm)
15	1.00	0.31	0.51	0.26	0.07
30	0.99	0.34	0.50	0.25	0.07

Table C.5. Integrated absorbance ratios of selected transitions in CH_3COCH_3:CH_3OH(1:5).

Temperature (K)	C=O stretch (5.847 μm)	CH_3 assym. deformation (7.053 μm)	CH_3 symm. deformation (7.335 μm)	CCC asymm. stretch (8.141 μm)	CO in-plane deformation (18.77 μm)
15	1.00	–	0.47	0.23	0.031
30	0.98	–	0.47	0.23	0.037
70	0.96	–	0.46	0.23	0.043
90	0.92	–	0.46	0.23	0.054
100	0.92	–	0.46	0.23	0.054
110	0.98	–	0.50	0.24	0.052
120	1.01	–	0.46	0.18	0.038
140	0.64	–	0.30	0.12	0.011

Table C.6. Integrated absorbance ratios of selected transitions in CH_3COCH_3:H_2O(1:20).

Temperature (K)	C=O stretch (5.847 μm)	CH_3 assym. deformation (7.053 μm)	CH_3 symm. deformation (7.335 μm)	CCC asymm. stretch (8.141 μm)	CO in-plane deformation (18.77 μm)
15	1.00	0.25	0.40	0.19	–
30	1.06	0.26	0.42	0.20	–
70	0.97	0.24	0.42	0.21	–
90	1.00	0.22	0.41	0.20	–
100	0.98	0.22	0.41	0.20	–
110	0.98	0.24	0.41	0.20	–
120	0.94	0.22	0.41	0.19	–
140	0.88	0.21	0.39	0.19	–

Table C.7. Integrated absorbance ratios of selected transitions in CH_3COCH_3:CO_2(1:20).

Temperature (K)	C=O stretch (5.847 μm)	CH_3 assym. deformation (7.053 μm)	CH_3 symm. deformation (7.335 μm)	CCC asymm. stretch (8.141 μm)	CO in-plane deformation (18.77 μm)
15	1.00	0.38	0.55	0.27	–
30	0.99	0.48	0.69	0.38	–
70	0.99	0.41	0.61	0.39	–
90	1.01	0.34	0.51	0.27	–
100	1.13	0.30	0.34	0.15	–

Table C.8. Integrated absorbance ratios of selected transitions in CH_3COCH_3:CO(1:20).

Temperature (K)	C=O stretch (5.847 μm)	CH_3 assym. deformation (7.053 μm)	CH_3 symm. deformation (7.335 μm)	CCC asymm. stretch (8.141 μm)	CO in-plane deformation (18.77 μm)
15	1.00	0.36	0.54	0.30	0.09
30	1.09	0.35	0.55	0.29	0.09

Table C.9. Integrated absorbance ratios of selected transitions in CH_3COCH_3:CH_3OH(1:20).

Temperature (K)	C=O stretch (5.847 μm)	CH_3 assym. deformation (7.053 μm)	CH_3 symm. deformation (7.335 μm)	CCC asymm. stretch (8.141 μm)	CO in-plane deformation (18.77 μm)
15	1.00	–	0.55	0.21	–
30	0.99	–	0.57	0.21	–
70	1.01	–	0.64	0.21	–
90	0.92	–	0.66	0.22	–
100	0.91	–	0.67	0.22	–
110	1.00	–	0.75	0.24	–
120	1.06	–	0.71	0.19	–
140	0.48	–	0.37	0.06	–

Table C.10. Integrated absorbance ratios of selected transitions in CH_3COCH_3:H_2O:CO_2(1:2.5:2.5).

Temperature (K)	C=O stretch (5.847 μm)	CH_3 assym. deformation (7.053 μm)	CH_3 symm. deformation (7.335 μm)	CCC asymm. stretch (8.141 μm)	CO in-plane deformation (18.77 μm)
15	1.00	0.43	0.56	0.28	0.07
30	1.00	0.42	0.56	0.27	0.07
70	0.98	0.40	0.56	0.26	0.05
90	0.97	0.38	0.54	0.24	–
100	0.92	0.36	0.51	0.23	–
110	0.90	0.35	0.50	0.23	–
120	0.89	0.32	0.48	0.22	–
140	0.58	0.20	0.33	0.18	–

Table C.11. Integrated absorbance ratios of selected transitions in CH_3COCH_3:H_2O:CO_2(1:10:10).

Temperature (K)	C=O stretch (5.847 μm)	CH_3 assym. deformation (7.053 μm)	CH_3 symm. deformation (7.335 μm)	CCC asymm. stretch (8.141 μm)	CO in-plane deformation (18.77 μm)
15	1.00	0.37	0.50	0.20	–
30	1.01	0.39	0.54	0.22	–
70	0.99	0.33	0.49	0.21	–
90	0.99	0.28	0.45	0.25	–
100	0.85	0.24	0.38	0.21	–
110	0.84	0.22	0.37	0.20	–
120	0.81	0.22	0.37	0.21	–
140	0.56	0.17	0.34	0.18	–

Table C.12. Integrated absorbance ratios of selected transitions in CH_3COCH_3:H_2O:CH_4(1:2.5:2.5).

Temperature (K)	C=O stretch (5.847 μm)	CH_3 assym. deformation (7.053 μm)	CH_3 symm. deformation (7.335 μm)	CCC asymm. stretch (8.141 μm)	CO in-plane deformation (18.77 μm)
15	1.00	0.32	0.49	0.26	0.09
30	1.00	0.30	0.48	0.26	0.08
70	1.04	0.47	0.47	0.24	0.06
90	1.05	0.27	0.46	0.23	0.05
100	1.05	0.25	0.44	0.23	0.04
110	1.04	0.24	0.23	0.23	0.05
120	1.02	0.23	0.44	0.23	0.07
140	0.51	0.11	0.22	0.13	0.05

Table C.13. Integrated absorbance ratios of selected transitions in CH_3COCH_3:H_2O:CH_4(1:10:10).

Temperature (K)	C=O stretch (5.847 μm)	CH_3 assym. deformation (7.053 μm)	CH_3 symm. deformation (7.335 μm)	CCC asymm. stretch (8.141 μm)	CO in-plane deformation (18.77 μm)
15	1.00	0.31	0.49	0.26	0.10
30	1.04	0.33	0.48	0.27	0.08
70	1.18	0.29	0.48	0.24	0.05
90	1.17	0.28	0.46	0.24	0.04
100	1.20	0.27	0.44	0.24	0.04
110	1.17	0.27	0.45	0.23	0.03
120	1.16	0.25	0.43	0.23	0.04
140	0.74	0.17	0.35	0.22	0.02

Table C.14. Integrated absorbance ratios of selected transitions in CH_3COCH_3:CO:CH_3OH(1:2.5:2.5).

Temperature (K)	C=O stretch (5.847 μm)	CH_3 assym. deformation (7.053 μm)	CH_3 symm. deformation (7.335 μm)	CCC asymm. stretch (8.141 μm)	CO in-plane deformation (18.77 μm)
15	1.00	–	0.43	0.22	0.022
30	0.97	–	0.43	0.22	0.029
70	0.87	–	0.41	0.22	0.050
90	0.86	–	0.41	0.23	0.051
100	0.85	–	0.41	0.23	0.047
110	0.80	–	0.41	0.19	0.041
120	0.80	–	0.40	0.19	0.037
140	0.24	–	0.13	0.05	0.022

Table C.15. Integrated absorbance ratios of selected transitions in CH_3COCH_3:CO:CH_3OH(1:10:10).

Temperature (K)	C=O stretch (5.847 μm)	CH_3 assym. deformation (7.053 μm)	CH_3 symm. deformation (7.335 μm)	CCC asymm. stretch (8.141 μm)	CO in-plane deformation (18.77 μm)
15	1.00	–	0.43	0.21	–
30	0.96	–	0.42	0.20	–
70	0.79	–	0.47	0.20	–
90	0.79	–	0.46	0.20	–
100	0.79	–	0.45	0.20	–
110	0.82	–	0.47	0.17	–
120	0.83	–	0.44	0.16	–
140	0.07	–	0.08	–	–